[23]W. D. Walker, Phys. Rev. Letters 24, 1143 (1970).
[24]*Handbook of Mathematical Functions*, edited by M. Abramowitz and I. Stegun (U.S. GPO, Washington, D.C., 1964).
[25]I. S. Gradshteyn and I. M. Ryzhik, *Tables of Integrals, Series, and Products* (Academic, New York, 1965).

PHYSICAL REVIEW D VOLUME 5, NUMBER 3 1 FEBRUARY 1972

Prospects for Producing and Detecting a Spinless W Boson in High-Energy Neutrino and Muon Experiments*

M. S. Turner† and B. C. Barish
California Institute of Technology, Pasadena, California 91109
(Received 24 September 1971)

We discuss here the possible production of the hypothetical spin-zero W boson (W_0) recently proposed by T. D. Lee, either through the decay of a directly produced spin-one W (W_1) or by direct production in the reactions $\nu+\mathrm{Fe}\rightarrow\mathrm{Fe}+W_0+\mu$ and $\mu+\mathrm{Fe}\rightarrow\mathrm{Fe}+W_0+\nu$. Theoretical cross sections and differential distributions are presented here for W_1 masses between 2 and 40 GeV/c^2 and W_0 masses between 2 and 8 GeV/c^2 for beam energies from 80 to 300 GeV. We show that assuming nonzero muon mass in the calculations for a neutrino beam, rather than zero muon mass as suggested by Lee, can increase the total theoretical cross section by up to a factor of 1000 if M_1 is greater than $4M_0$ or if the W_1's anomalous magnetic moment is near 1. In general, the production cross sections with incident neutrinos for W_0's are down from those for W_1's by a factor of 20–100, while the cross sections with incident muons are nearly equal. The effects of the W_1's anomalous magnetic moment, W_0 and W_1 mass, and incident energy upon cross sections and distributions are discussed for the coherent and incoherent cases. Possible signatures for detecting a W_0 either in the decay of a W_1 or in a q^2-ν plot in direct production are discussed.

I. INTRODUCTION

In one of a recent series of papers on the weak and electromagnetic interactions (in order to make the weak interaction renormalizable), Lee[1] has hypothesized a spinless W boson of opposite metric, in addition to the usual spin-one W boson.

Eventually, with only a spin-one W, cross sections would exceed the unitarity bound in first order. The propagator for a massive particle of spin one is[2]

$$\frac{-\delta_{\mu\nu}+q_\mu q_\nu/M^2}{q^2-M^2}\,. \tag{1}$$

The $q_\mu q_\nu$ term, which is not present in the propagator of a massless spin-one particle (i.e., a photon), is what makes renormalization of the weak interactions impossible. As $|q^2|$ increases, the term

$$\frac{q_\mu q_\nu/M^2}{q^2-M^2} \tag{2}$$

begins to go like a constant, instead of falling with $|q^2|$.

The effect of introducing an additional spinless W is to change the W propagator and the $W_\nu\rightarrow W_\mu\gamma$ electromagnetic vertex function everywhere. The propagator becomes[1]

$$\frac{-\delta_{\mu\nu}}{q^2-M_1^{\,2}}+\frac{q_\mu q_\nu}{M_1^{\,2}}\left(\frac{1}{q^2-M_1^{\,2}}-\frac{1}{q^2-M_0^{\,2}}\right), \tag{3}$$

where M_1 is the mass of the spin-one W (W_1) and M_0 is the mass of the spinless W (W_0). The minus sign between the W_1 and W_0 propagators is what is meant by opposite metric and is crucial. The W_0 couples to the divergence of the weak current, as is necessary for relativistically invariant amplitudes. Now, the former bothersome $q_\mu q_\nu$ term goes as

$$\frac{q_\mu q_\nu(M_1^{\,2}-M_0^{\,2})}{M_1^{\,2}(q^2-M_1^{\,2})(q^2-M_0^{\,2})}, \tag{4}$$

and for large $|q^2|$'s vanishes as $1/|q^2|$. The W_0 fixes up weak-interaction theory so that it mimics electromagnetic-interaction theory and is renormalizable.

In this paper we address ourselves to the possible detection of a W_0, if it exists. Present experiments at the National Accelerator Laboratory (NAL) are expected to search for the W_1 and it is possible that it will be directly produced and detected at the energies available there. If not, it is still possible that the effect of the W propagator will be seen, for example, in high-energy deep-inelastic neutrino scattering. A natural question is whether it is possible to also observe a W_0 in similar experiments.

The effect of the W_0 on inelastic neutrino scattering is far less pronounced than that of the W_1. At the large $|q^2|$'s soon to be available at NAL, a damping of cross section due to the propagator of a massive W_1 could be observed. The additional presence of a W_0 would cause only a very small perturbation on the W_1 propagator, a perturbation that is not easily seen except at extremely high energies. The $q_\mu q_\nu$ term, where the perturbation occurs, is down by a factor of m_l/M_1^2 because, when the weak current is coupled to the propagator, the q_μ brings out a factor of the lepton mass as follows:

$$q_\mu[\overline{u}_l \gamma_\mu (1-\gamma_5)u_\nu] \tag{5a}$$

is, upon substituting $q_\mu = p_\nu - p_l$, equal to

$$-\overline{u}_l \not{p}_l (1-\gamma_5)u_\nu + \overline{u}_l (1+\gamma_5)\not{p}_\nu u_\nu , \tag{5b}$$

which reduces to

$$-m_l \overline{u}_l (1-\gamma_5)u_\nu . \tag{5c}$$

The possibility of seeing the effect of a W_0 on muon- or neutrino-induced W_1 production is likewise precluded. Searching for a W_0 through its effects on the W propagator is at least a step beyond seeing the effects of a W_1.

It appears then that the only real hope for a W_0 search is through actually producing them. There are many ways to produce a W_0 directly, such as in nucleon-nucleon reactions, with colliding electron-positron beams, with muons or neutrinos, and from the decay of a W_1 if the W_0 is less massive than a W_1. The case of W_1 decay will be discussed first, since it offers the most copious production of W_0's for most values of M_0 and M_1. Then, direct production with muon and neutrino beams will be discussed in detail. Total cross sections and differential distributions will be presented for iron for various W_0 and W_1 masses and energies.

II. THE DECAY $W_1 \to W_0 + \gamma$

In order to calculate the rate for $W_1 \to W_0 + \gamma$ and other processes, a vertex function is needed for $W_\nu \to W_\mu + \gamma$. In Ref. 1 Lee proposed the following nonunique function which satisfies current conservation and is in accordance with the principle of minimal electromagnetic interaction:

$$\begin{aligned} V_\lambda(k', k)_{\mu\nu} = e[&\delta_{\mu\nu}(k+k')_\lambda \\ &+ (M_1^2/M_0^2 + \kappa)(\delta_{\lambda\mu}k_\nu + \delta_{\lambda\nu}k'_\mu) \\ &- (1+\kappa)(\delta_{\lambda\mu}k'_\nu + \delta_{\lambda\nu}k_\mu)] , \end{aligned} \tag{6}$$

where k is the initial four-momentum, k' is the final four-momentum, ν is the initial W index, μ is the final W index, λ is the photon index, the W_1 couples by its polarization four-vector and the W_0 through its four-momentum divided by M_1, and κ is the anomalous magnetic moment of the W_1. The anomalous quadrupole moment is assumed to be zero. Except for the term in $(M_1/M_0)^2$, this vertex function is identical to the usual one for $W_1 \to W_1 + \gamma$. For $M_1 > M_0$ the amplitude for the decay $W_1 \to W_0 + \gamma$ is

$$V_\lambda(k', k)_{\mu\nu} e^*_\lambda \frac{k'_\mu}{M_1} \eta_\nu , \tag{7}$$

where η_ν is the polarization of the initial W_1 and e_λ is the polarization of the photon. The rate is then

$$\Gamma(W_1 \to W_0\gamma) = \tfrac{1}{24}\alpha(1-\kappa)^2(M_1^2 - M_0^2)^3/M_1^5 , \tag{8}$$

where α is the fine-structure constant $\frac{1}{137}$.

The W_0 itself must then decay hadronically. $W_0 \to l\nu$ is practically forbidden, since the W_0 is spinless and hence both the lepton and neutrino cannot be left-handed as is strongly favored (the W_0 is like a heavy π trying to decay). If $M_0 > M_1$, the W_0 can decay leptonically indirectly by $W_0 \to W_1 + \gamma \to l + \nu + \gamma$.

If the $W_1 \to W_0\gamma$ decay rate is large compared to $W_1 \to l\nu$, the W_1 must be detected through nonleptonic decay channels. The rate for $W_1 \to l\nu$ (in the limit of zero lepton mass) is easily calculated to be

$$\Gamma(W_1 \to l\nu) = \frac{G}{\sqrt{2}}\frac{1}{3\pi}M_1^3 \tag{9}$$

for both lepton modes added together. G is the weak-interaction coupling constant ($\approx 10^{-5}/M_N^2$).

Contours of

$$\frac{\text{Rate}(W_1 \to l\nu)}{\text{Rate}(W_1 \to W_0\gamma)} = \frac{4\sqrt{2}}{\pi\alpha}\frac{1}{(1-\kappa)^2}\frac{GM_1^2}{[1-(M_0/M_1)^2]^3} \tag{10}$$

are shown in Fig. 1. For W_1 masses less than 20 GeV/c^2, W_0 masses less than 7 GeV/c^2, and $\kappa = 0$, the ratio is less than 1 and the decay mode $W_1 \to W_0\gamma$ will dominate. If $\kappa = 1$, the $W_1 \to W_0\gamma$ mode is forbidden. If κ is negative, then $W_1 \to W_0\gamma$ is more favorable, since the κ dependence in the branching ratio is

$$1/(1-\kappa)^2 . \tag{11}$$

If the W_1 decays frequently via this channel

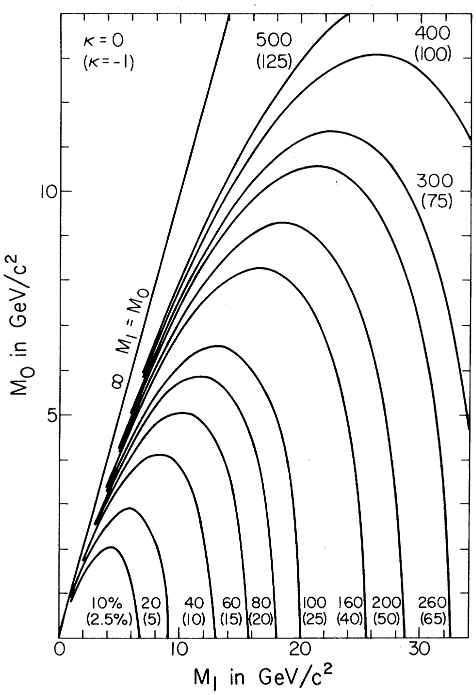

FIG. 1. Contours of the ratio $\Gamma(W_1 \to l\nu)/\Gamma(W_1 \to W_0\gamma)$ (in percent) as a function of M_0 and M_1. For $M_1 < 20$ GeV/c^2, $M_0 < 7$ GeV/c^2, and $\kappa = 0$, the decay mode $W_1 \to W_0\gamma$ dominates. The ratio varies as $(1-\kappa)^{-2}$ and the numbers in parentheses are for $\kappa = -1$ (for $\kappa = 1$, $W_1 \to W_0\gamma$ is forbidden).

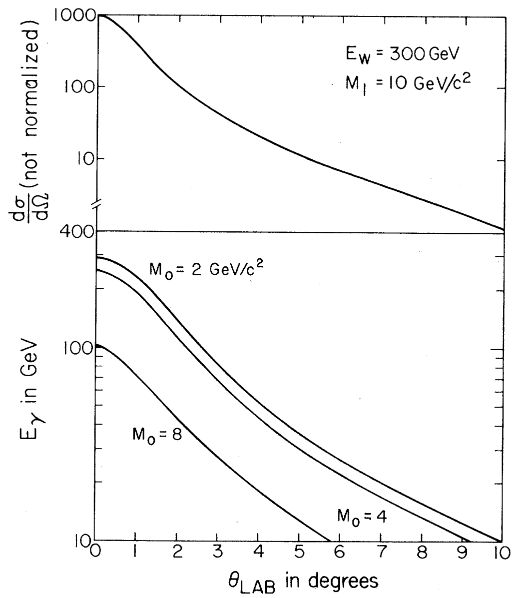

FIG. 2. E_γ and $d\sigma/d\Omega$ (not normalized) as a function of lab angle, for the decay of a 300-GeV, 10-GeV/c^2 mass, and left-handed W_1 ($W_1 \to W_0\gamma$), and M_0's of 2, 4, and 8 GeV/c^2. As M_0 varies, the E_γ vs lab-angle curve moves up or down ($d\sigma/d\Omega$ vs lab angle is unaffected). Changing the ratio of W_1 energy to mass moves the energy-angle curve up or down and compresses or expands the angles scale approximately linearly (expands as the ratio increases) for both curves.

($W_0\gamma$), could the uniqueness of this decay be used to infer the existence of a W_0? A comparison of the production cross sections for the W_1 and W_0 (Sec. III) makes it attractive to consider using the W_1 decay channel to detect a W_0. The signature in this case is a wide-angle high-energy γ ray. Figure 2 shows a plot of the laboratory energy vs laboratory angle and $d\sigma/d\Omega$ (not normalized) vs laboratory angle for γ rays from the decay of a 10-GeV/c^2 W_1 with lab energy of 300 GeV polarized left-handed. (Note: W_1's produced from neutrinos tend to be left-handed and carry away most of the beam energy; the reason for this will be discussed later.) Therefore, if photon distributions could be detected and both the W_1 and W_0 existed, with the W_1 heavier, one would expect a clustering of photons along one of the lines in the energy-vs-angle plot.

III. DIRECT PRODUCTION WITH MUONS AND NEUTRINOS

Incident Neutrinos

W_0's can be produced directly in a process identical to W_1 production with either muons or neutrinos. The two first-order Feynman diagrams for neutrino-induced W_0 production are illustrated in Figs. 3(a) and 3(b). Figure 3(a) represents the process in which there is an off-mass-shell muon propagating and Fig. 3(b) the process in which a W propagates. In W_1-production diagram 3(a) dominates because of the denominator in the muon propagator. Diagram 3(b) never becomes large since the denominator of the propagator involved can never get smaller than the mass squared of the W_1. Therefore, diagram 3(b) is unimportant for W_1 production (except at very high energies).

In the case of W_0 production, diagram 3(a) is suppressed for the reason that a W_0 cannot decay into leptons. Algebraically this is easy to show. Let ν, μ, W, p_0, and p be, respectively, the four-momenta of the neutrino, the muon, the W_0, the incoming target, and the outgoing target. Also, let $q = p - p_0$, $P = p + p_0$, and v represent the electromagnetic current of the target. Then the amplitude for diagram 3(a) is

$$-\frac{e^2g}{M_1q^2}\,\bar{u}_\mu \not{v}\, \frac{(\not{q}+\not{\mu}+m_\mu)\not{W}}{(\mu+q)^2-m_\mu^2}\,(1-\gamma_5)u_\nu\,, \tag{12}$$

which is equal to

$$+\frac{e^2g}{M_1q^2}\,\bar{u}_\mu \not{v}\, \frac{(\not{\mu}+\not{q}+m_\mu)(\not{\mu}+\not{q})}{(\mu+q)^2-m_\mu^2}\,(1-\gamma_5)u_\nu \tag{13}$$

as $W=\nu-\mu-q$, and expression (12) finally reduces to

$$\frac{e^2 g}{q^2 M_1}\bar{u}_\mu \not{p}\frac{[m_\mu{}^2+m_\mu(\not{\mu}+\not{q})](1-\gamma_5)}{(\mu+q)^2-m_\mu{}^2}u_\nu + \frac{e^2 g}{q^2 M_1}\bar{u}_\mu \not{p}(1-\gamma_5)u_\nu\,, \tag{14}$$

where g is related to the Fermi constant by $g^2=GM_1{}^2/\sqrt{2}$. The second term diverges as q^2 goes to zero and is canceled by a similar term of opposite sign from diagram 3(b). The effect of the muon pole which had caused diagram 3(a) to dominate in W_1 production is now suppressed by a factor of the lepton mass. In his paper speculating about the existence of a W_0,[1] Lee suggests neglecting the muon mass (i.e., ignoring the muon pole). This assumption, as will be seen later, is not always such a good one for W_0 production with neutrinos. All terms have been kept for our calculations.

The amplitude for diagram 3(b) is easy to write; it is

$$\frac{e^2 g}{q^2 M_1}\bar{u}_\mu\gamma_\alpha(1-\gamma_5)u_\nu\left[\frac{\delta_{\alpha\nu}}{(q+W)^2-M_1{}^2}-\frac{(q+W)_\alpha(q+W)_\nu}{M_1^2}\left(\frac{1}{(q+W)^2-M_1{}^2}-\frac{1}{(q+W)^2-M_0{}^2}\right)\right]V_\beta(W,q+W)_{\mu\nu}\,W_\mu v_\beta\,. \tag{15}$$

It is a straightforward but tedious job to show that when diagrams 3(a) and 3(b) are taken together they conserve current.

Since the kinematics are identical and the matrix element is similar to that for W_1 production, the procedures chosen here parallel those of Wu and Yang[3] and are detailed in the Appendix.

For a neutron or proton target the usual SLAC dipole-fit form factors are used.[4] In addition, in order to calculate the cross sections for neutrons and protons bound in a nucleus, a statistical factor has been included. This factor takes into account the fact that for small momentum transfers (ones where $|\vec{q}|$ is less than twice the Fermi momentum) not all the nucleons in the target can undergo such a change in momentum, since it would not take some of them outside of the Fermi sphere (as it must in accordance with the Pauli exclusion principle). The exclusion-principle correction factor is then[5]

$$R(|q|^2)=\frac{3}{2}\frac{|\vec{q}|}{2Q_F}-\frac{1}{2}\left(\frac{|\vec{q}|}{2Q_F}\right)^3 \quad \text{for} \quad |\vec{q}|<2Q_F \tag{16}$$

$$=1 \qquad \text{for} \quad |\vec{q}|\geq 2Q_F\,, \tag{17}$$

where Q_F is the Fermi momentum $0.284m_p$ and $|\vec{q}|$ is evaluated in the lab frame. (For simplicity, it is assumed that initially all the nucleons are at rest.) Neglecting the initial Fermi motion of the nucleons tends only to make the threshold dependence of the neutron and proton cross sections somewhat too steep.

In calculating the coherent cross section for W_0 production, the aforementioned statistical factor is not used, the form factor for an exponential charge distribution[6] is used (the magnetic form factor is set equal to zero), the target mass is set equal to 10^{10} proton masses (to simulate a stationary target, although the cross section varies only a few percent between using the mass of the nucleus and 10^{10} proton masses), and finally $|t|$'s ($t=q^2$) greater than 0.25 GeV^2 are forbidden to ensure coherence (i.e., the nucleus does not break up).

To obtain cross sections, numerical integrations were done over two variables, $|\alpha|$ $[\alpha=(\nu\cdot q)]$ and $|t|$. The $|\alpha|$ integration was done using a ten-point Simpson's algorithm. The $|t|$ integration was done using a modified Simpson algorithm with the points being chosen in a geometric progression to smooth out the $|t|$ dependence, which is approximately exponential. The numerical accuracy for the integrations is 5%. To calculate a set of three cross sections (neutron, proton, and coherent), approximately 20 sec of compute time on an IBM 370/155 was required. The total cross sections have been checked against Monte Carlo integrations of

$$\frac{d\sigma}{d|t|d|\alpha|d\xi\, d\phi_+}$$

(see the Appendix for definitions of ξ and ϕ_+). The cross sections with m_μ set equal to zero agree to within 3% of similar calculations by Linsker.[7] Our calculations with the nonzero muon-mass matrix element are in perfect agreement, when the muon mass is externally set equal to zero, with the calculations using a matrix element assuming zero muon mass from the outset. Our results both with nonzero muon mass and zero muon mass are in serious disagreement with calculations done by Reiff.[8] The differences in the calculations are not apparent.

The total cross section per proton on an iron (Fe^{56}) target is

$$\sigma_T=\sigma_p+[(A-Z)/Z]\,\sigma_n+\sigma_{\text{coherent}}\,, \tag{18}$$

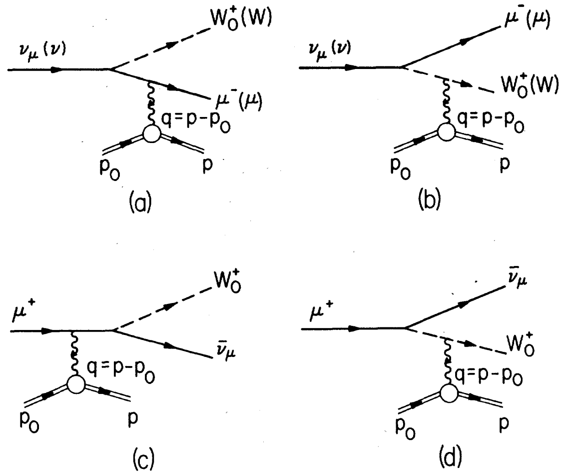

FIG. 3. Feynman first-order diagrams for W_0 production with neutrinos [3(a) and 3(b)] and muons [3(c) and 3(d)]. Diagram 3(a) is important only if $M_1 > 4M_0$ or $\kappa=1$ [otherwise diagram 3(b) dominates] and diagram 3(d) always dominates.

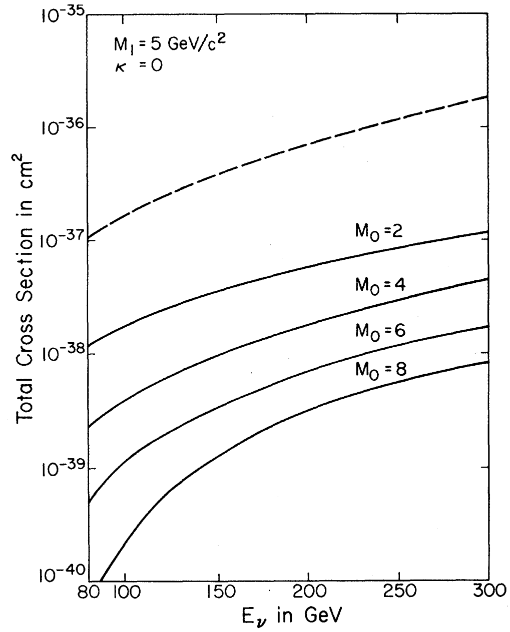

FIG. 4. W_1 (dashed line) and W_0 (solid lines) total production cross sections (per proton) by neutrinos on iron vs neutrino energy. Here $M_1 = 5$ GeV/c^2, $\kappa=0$, and $M_0=2$, 4, 6, and 8 GeV/c^2. W_0 production is down from W_1 production by a factor of 20–100.

where σ_n and σ_p are the corrected cross sections for neutron and proton, respectively, and σ_{coherent} is the coherent cross section on iron per proton.

In order to compare W_0 and W_1 production, it is necessary to adopt some conventions. When comparing quantities that are kinematical, such as differential distributions, the important point in comparison is to use the same mass for the produced particle (i.e., M_0 in the W_0 case should be equal to M_1 in the W_1 case). For comparing cross sections, it is most useful to use the same M_1 in W_1 production and in W_0 production and vary M_0, since if the W_1 exists, that fixes M_1, but M_0 is still an independent parameter. For a grand comparison, M_0 can be set equal to M_1 for W_0 production and then the results can be compared to W_1 production for that same M_1. This way the kinematics and the dynamics are as similar as possible.

In general, the W_0 total cross sections are down by a factor of 20–100 for fixed W_1 mass (depending upon the W_0 mass) from W_1 total cross sections, as can be seen in Figs. 4–6.[9] However, for large W_1 masses the cross sections for relatively light W_0's can be equal to or even greater than the W_1 cross sections, as is apparent in Fig. 6, where M_1 is 15 GeV/c^2. In these cases W_1 production is suppressed since the process is barely above threshold. The total cross sections decrease with increasing W_0 mass, roughly a factor of 2–3 for each additional 2 GeV/c^2 of W_0 mass. Reiff found that when well above threshold the nucleon cross sections increased with increasing W_0 mass[8]; no such behavior was observed in these calculations.

Just as in W_1 production, the neutron and proton cross sections rise sharply near threshold and level off quickly. The correction for Fermi statistics amounts at most to a 20% reduction in incoherent cross section. Again, as in W_1 production the coherent cross section takes much longer to reach its plateau because the process must get well above threshold in order that $|t|$ be small enough so that the sharp nuclear form factor does not completely eliminate the coherent process.

The Muon Mass

Figures 7 and 8 show the total cross section per proton on iron for fixed W_0 mass and varying energy, both for zero and nonzero muon mass for several values of W_1 mass and $\kappa=0$. Significant differences occur between the two cases for W_1 mass greater than 4 times the W_0 mass. In these cases neglecting the muon mass results in total cross sections low by up to a factor of 1000. The explanation is simple. If it were not for the factor of the muon mass suppressing the muon pole, the diagram with the muon propagator [diagram 3(a)] would dominate as in the case of W_1 production. Because of this damping, the diagram with the W propagator [diagram 3(b)] usually dominates. For large W_1 masses the propagator goes just like $1/M_1^2$ (the factor of M_1 in the coupling constant g

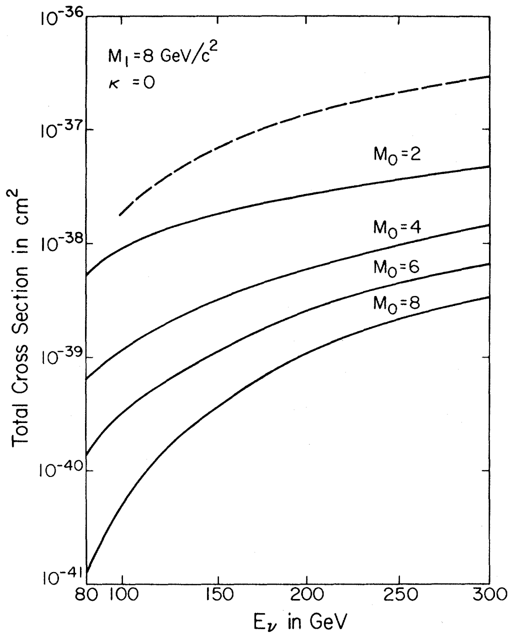

FIG. 5. Same as Fig. 4, but with $M_1 = 8$ GeV/c^2.

is canceled by the $1/M_1$ in the coupling of the W_0), so the amplitude falls off sharply with increasing M_1. Eventually the muon pole, although down by a factor of m_μ, begins to dominate. In order for this to occur, M_1 must be large and M_0 must be small enough so that kinematically the process can get close to the muon pole [i.e., small $(\mu + q)^2$'s]. The finite muon mass tends to ease

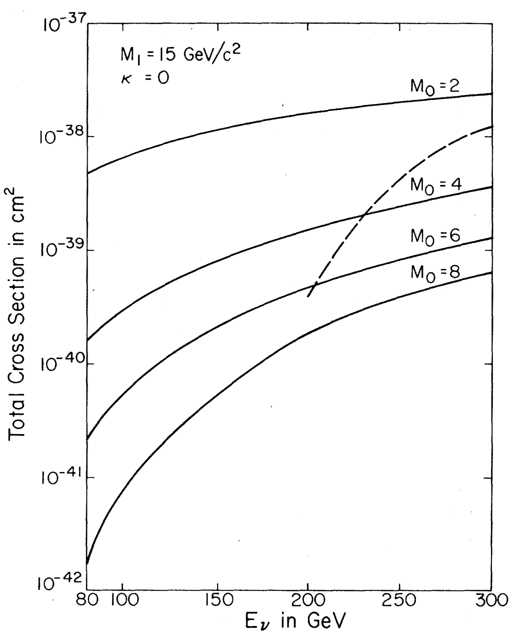

FIG. 6. Same as Fig. 4, but with $M_1 = 15$ GeV/c^2. Here W_0 production exceeds W_1 production for small W_0 masses since W_1 is still near threshold.

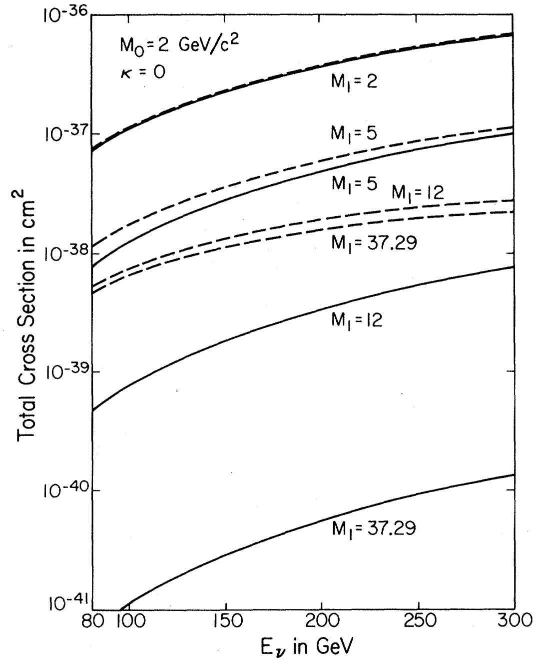

FIG. 7. W_0 total production cross sections (per proton) by neutrinos on iron with $m_\mu = 0$ (solid lines) and $m_\mu \neq 0$ (dashed lines) vs neutrino energy. Here $M_0 = 2$ GeV/c^2, $\kappa = 0$, and $M_1 = 2$, 5, 12, and 37.29 GeV/c^2. For $M_1 > 4M_0$, the assumption of $m_\mu = 0$ is a poor one.

the dependence upon the W_1 mass when the W_1 mass is many times greater (≈ 4 or more) than the W_0 mass by greatly enhancing the coherent pro-

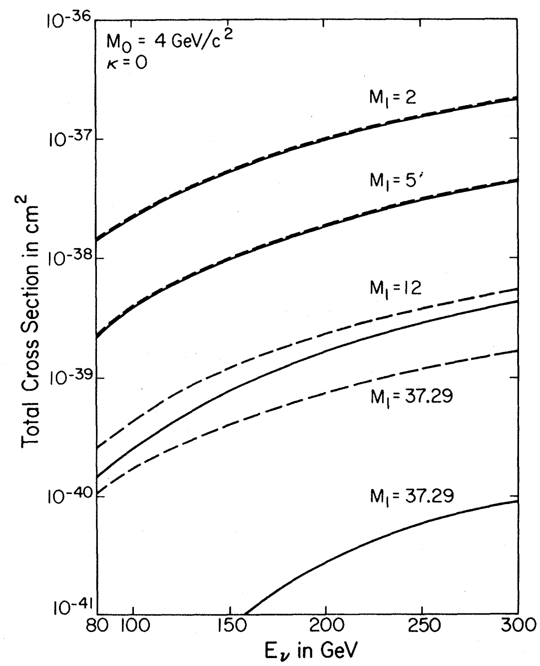

FIG. 8. Same as Fig. 7, but with $M_0 = 4$ GeV/c^2.

TABLE I. Theoretical W_0-production cross sections by neutrinos and muons on iron for $M_1=5$ GeV/c^2, $\kappa=0$, and $M_0=2$, 4, 6, and 8 GeV/c^2 in units of 10^{-38} cm^2 per proton. σ_p denotes the cross section of a proton for W_0 production, σ_n' denotes $(A-Z)/Z$ times the cross section of a neutron for W_0 production, σ_c denotes the coherent cross section of an iron nucleus per proton, and σ_T denotes the total W_0-production cross section per proton [cf. Eq. (18)]. The cross sections not in parentheses are for incident neutrinos and $m_\mu \neq 0$; the cross sections in parentheses are for incident neutrinos and $m_\mu=0$. To obtain the cross sections for incident muons it is only necessary to divide the numbers in parentheses by 2.

				$M_1=5$ GeV/c^2				
M_0	σ_n'	σ_p	σ_c	σ_T	σ_n'	σ_p	σ_c	σ_T
		E_ν (E_μ) = 80 GeV				E_ν (E_μ) = 100 GeV		
2	0.116 (0.099)	0.418 (0.396)	0.595 (0.306)	1.13 (0.801)	0.157 (0.135)	0.589 (0.566)	0.975 (0.576)	1.72 (1.28)
4	0.056 (0.049)	0.153 (0.153)	0.014 (0.013)	0.223 (0.215)	0.087 (0.076)	0.255 (0.256)	0.041 (0.040)	0.384 (0.372)
6	0.016 (0.014)	0.035 (0.036)	2.55×10^{-4} (2.63×10^{-4})	0.051 (0.050)	0.034 (0.030)	0.080 (0.080)	1.35×10^{-3} (1.39×10^{-3})	0.114 (0.111)
8	1.75×10^{-3} (1.55×10^{-3})	3.41×10^{-3} (3.51×10^{-3})	5.98×10^{-7} (6.53×10^{-7})	5.16×10^{-3} (5.06×10^{-3})	7.05×10^{-3} (6.22×10^{-3})	0.014 (0.015)	1.85×10^{-5} (1.95×10^{-5})	0.022 (0.021)
		E_ν (E_μ) = 200 GeV				E_ν (E_μ) = 300 GeV		
2	0.362 (0.313)	1.52 (1.49)	3.90 (3.05)	5.78 (4.85)	0.549 (0.472)	2.45 (2.41)	8.09 (6.90)	11.1 (9.78)
4	0.262 (0.228)	0.927 (0.929)	0.604 (0.601)	1.79 (1.76)	0.432 (0.374)	1.69 (1.69)	2.02 (2.03)	4.14 (4.09)
6	0.164 (0.143)	0.487 (0.489)	0.072 (0.074)	0.723 (0.706)	0.311 (0.270)	1.05 (1.05)	0.412 (0.420)	1.77 (1.74)
8	0.086 (0.075)	0.217 (0.218)	6.67×10^{-3} (6.85×10^{-3})	0.310 (0.300)	0.203 (0.176)	0.588 (0.590)	0.066 (0.067)	0.857 (0.833)

TABLE II. Same as Table I but with $M_1=8$ GeV/c^2.

				$M_1=8$ GeV/c^2				
M_0	σ_n'	σ_p	σ_c	σ_T	σ_n'	σ_p	σ_c	σ_T
		E_ν (E_μ) = 80 GeV				E_ν (E_μ) = 100 GeV		
2	0.036 (0.028)	0.140 (0.103)	0.434 (0.060)	0.610 (0.190)	0.051 (0.040)	0.196 (0.156)	0.644 (0.116)	0.891 (0.312)
4	0.016 (0.014)	0.043 (0.041)	5.22×10^{-3} (2.73×10^{-3})	0.065 (0.057)	0.027 (0.023)	0.076 (0.072)	0.014 (8.47×10^{-3})	0.116 (0.104)
6	4.28×10^{-3} (3.73×10^{-3})	9.39×10^{-3} (9.34×10^{-3})	6.70×10^{-5} (5.77×10^{-5})	0.014 (0.013)	9.78×10^{-3} (8.51×10^{-3})	0.023 (0.023)	3.51×10^{-4} (3.09×10^{-4})	0.033 (0.031)
8	4.24×10^{-4} (3.80×10^{-4})	8.27×10^{-4} (8.54×10^{-4})	1.41×10^{-7} (1.22×10^{-7})	1.25×10^{-3} (1.23×10^{-3})	1.90×10^{-3} (1.69×10^{-3})	3.86×10^{-3} (3.94×10^{-3})	4.23×10^{-6} (4.10×10^{-6})	5.76×10^{-3} (5.63×10^{-3})
		E_ν (E_μ) = 200 GeV				E_ν (E_μ) = 300 GeV		
2	0.134 (0.112)	0.533 (0.482)	1.88 (0.688)	2.55 (1.28)	0.220 (0.187)	0.913 (0.856)	3.37 (1.68)	4.50 (2.72)
4	0.096 (0.083)	0.317 (0.312)	0.180 (0.144)	0.593 (0.539)	0.174 (0.151)	0.627 (0.622)	0.598 (0.525)	1.40 (1.30)
6	0.060 (0.052)	0.168 (0.168)	0.020 (0.019)	0.247 (0.239)	0.126 (0.110)	0.397 (0.397)	0.117 (0.114)	0.640 (0.621)
8	0.031 (0.027)	0.074 (0.075)	1.79×10^{-3} (1.81×10^{-3})	0.107 (0.104)	0.082 (0.071)	0.225 (0.227)	0.019 (0.019)	0.326 (0.318)

TABLE III. Same as Table I but with $M_1 = 15$ GeV/c^2 and in units of 10^{-40} cm^2 per proton.

	$M_1 = 15$ GeV/c^2							
M_0	σ'_n	σ_p	σ_c	σ_T	σ'_n	σ_p	σ_c	σ_T
	E_ν (E_μ) = 80 GeV				E_ν (E_μ) = 100 GeV			
2	0.914 (0.401)	5.66 (1.22)	42.4 (0.560)	49.0 (2.18)	1.16 (0.624)	6.85 (1.95)	60.4 (1.11)	68.4 (3.69)
4	0.282 (0.192)	0.951 (0.487)	0.365 (0.027)	1.60 (0.706)	0.450 (0.348)	1.52 (0.921)	0.885 (0.085)	2.86 (1.35)
6	0.065 (0.051)	0.155 (0.109)	2.74×10^{-3} (5.53×10^{-4})	0.223 (0.161)	0.147 (0.126)	0.362 (0.284)	0.012 (3.29×10^{-3})	0.521 (0.413)
8	5.62×10^{-3} (4.85×10^{-3})	0.011 (9.42×10^{-3})	6.98×10^{-6} (7.51×10^{-7})	0.017 (0.014)	0.026 (0.024)	0.054 (0.047)	1.18×10^{-4} (5.15×10^{-5})	0.080 (0.071)
	E_ν (E_μ) = 200 GeV				E_ν (E_μ) = 300 GeV			
2	2.79 (2.19)	13.7 (7.39)	144 (7.24)	160 (16.8)	4.87 (4.22)	22.0 (14.9)	216 (19.0)	243 (38.1)
4	1.75 (1.63)	5.91 (4.91)	7.16 (1.59)	14.8 (8.12)	3.58 (3.45)	12.3 (11.1)	18.2 (6.24)	34.1 (20.8)
6	1.05 (1.01)	2.89 (2.68)	0.461 (0.215)	4.40 (3.90)	2.55 (2.51)	7.57 (7.27)	2.33 (1.42)	12.5 (11.2)
8	0.517 (0.508)	1.23 (1.19)	0.031 (0.021)	1.78 (1.72)	1.63 (1.61)	4.26 (4.19)	0.310 (0.248)	6.20 (6.05)

TABLE IV. Same as Table I but with $M_1 = 37.29$ GeV/c^2 and in units of 10^{-40} cm^2 per proton.

	$M_1 = 37.29$ GeV/c^2							
M_0	σ'_n	σ_p	σ_c	σ_T	σ'_n	σ_p	σ_c	σ_T
	E_ν (E_μ) = 80 GeV				E_ν (E_μ) = 100 GeV			
2	0.577 (0.011)	4.78 (0.038)	43.3 (0.015)	48.9 (0.064)	0.612 (0.018)	5.33 (0.063)	61.7 (0.031)	67.6 (0.111)
4	0.118 (5.26×10^{-3})	0.560 (0.015)	0.372 (7.42×10^{-4})	1.05 (0.021)	0.141 (9.94×10^{-3})	0.739 (0.030)	0.887 (2.39×10^{-3})	1.77 (0.042)
6	0.023 (1.35×10^{-3})	0.066 (3.33×10^{-3})	2.61×10^{-3} (1.54×10^{-5})	0.091 (4.70×10^{-3})	0.036 (3.52×10^{-3})	0.118 (9.04×10^{-3})	0.011 (9.10×10^{-5})	0.165 (0.013)
8	1.75×10^{-3} (1.24×10^{-4})	3.74×10^{-3} (2.77×10^{-4})	7.33×10^{-6} (1.02×10^{-6})	$5.5\ \times10^{-3}$ (4.02×10^{-4})	5.66×10^{-3} (6.33×10^{-4})	0.013 (1.46×10^{-3})	1.03×10^{-4} (1.12×10^{-6})	0.019 (2.09×10^{-3})
	E_ν (E_μ) = 200 GeV				E_ν (E_μ) = 300 GeV			
2	0.768 (0.075)	7.16 (0.275)	144 (0.211)	152 (0.561)	0.929 (0.167)	8.45 (0.622)	208 (0.576)	217 (1.37)
4	0.236 (0.056)	1.43 (0.185)	6.36 (0.047)	8.03 (0.288)	0.345 (0.137)	2.02 (0.472)	13.9 (0.194)	16.3 (0.803)
6	0.102 (0.034)	0.424 (0.101)	0.316 (6.58×10^{-3})	0.842 (0.142)	0.189 (0.099)	0.784 (0.312)	1.24 (0.045)	2.21 (0.456)
8	0.043 (0.017)	0.131 (0.044)	0.014 (6.74×10^{-4})	0.188 (0.062)	0.105 (0.063)	0.339 (0.179)	0.105 (8.11×10^{-3})	0.549 (0.250)

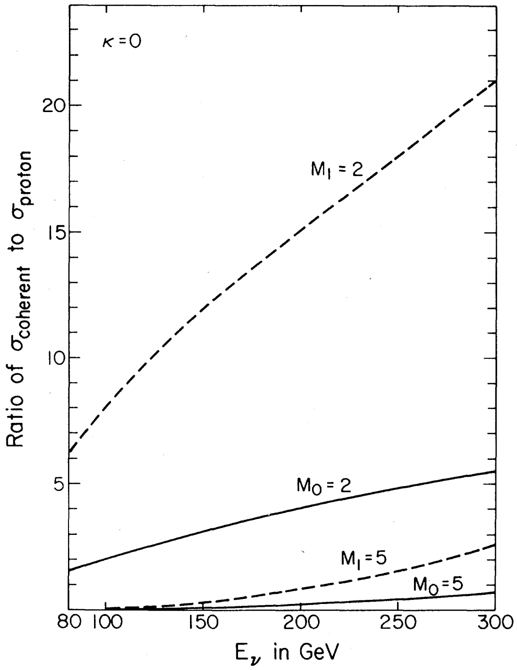

FIG. 9. Ratio of coherent cross section to proton cross section for neutrino-induced W_1 (dashed lines) and W_0 production (solid lines) off iron as a function of neutrino energy. Here $M_1 = 2$ and 5 GeV/c^2 for W_1 production, $M_1 = M_0 = 2$ and 5 GeV/c^2 for W_0 production, and $\kappa = 0$. Except where the muon pole dominates in W_0 production, the coherent process is not dominant.

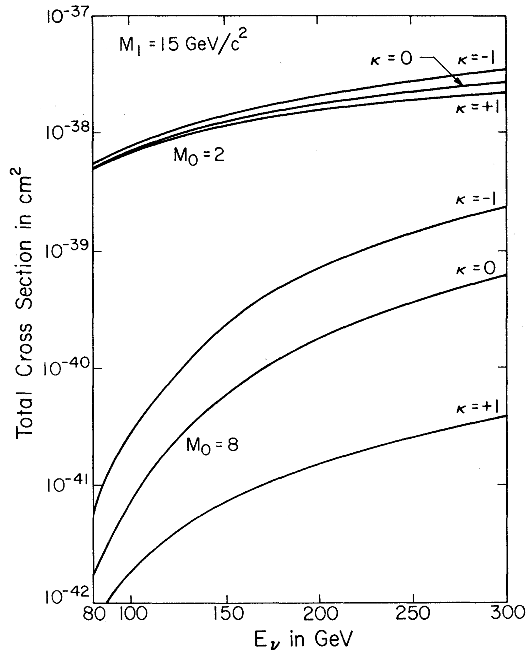

FIG. 10. W_0 total production cross sections (per proton) by neutrinos on iron for $M_1 = 15$ GeV/c^2, $M_0 = 2$ and 8 GeV/c^2, and $\kappa = -1$, 0, and 1 vs neutrino energy. Except where the muon pole dominates ($M_1 > 4M_0$), the κ dependence is severe.

cess and making it dominant, at the same time affecting nucleon cross sections much less critically. When the muon pole is not dominant (i.e., M_1 and M_0 are relatively the same size), the cross sections computed with $m_\mu \neq 0$ can be slightly less (at most 10%) than those computed with $m_\mu = 0$ for proton and coherence. Here, apparently diagram 3(a) interferes destructively, causing a slight decrease in cross section. Tables I–IV contain σ_p, σ_n, σ_{coherent}, and σ_T for various W_1 and W_0 masses and beam energies for zero and nonzero muon mass.[10]

In W_1 production, when the process gets well above threshold it is the coherent cross section that gets large and contributes the most to the total cross section. As the neutrino energy increases, the coherent process can get larger as smaller $|t|$'s are permitted and the process is then less suppressed by the sharp nuclear form factor. In W_0 production, except where the muon pole comes into play, the coherent process never really dominates as in W_1 production. Figure 9 shows this clearly by comparing the ratio of coherent cross section to proton cross section in W_1 production[11] with W_0 production in a region where the muon pole is negligible.

For fixed M_0 and M_1, as the beam energy increases, the cross sections for zero and nonzero muon mass become equal. The reason for this is as follows: As the beam energy increases, the ranges of $(\mu + q)^2$ and $(q + W)^2$ increase. Eventually, the region where the muon propagator is much larger than the W propagator [small $(\mu + q)^2$'s as compared to small $(q + W)^2$'s] becomes insignificant compared to the entire range of $(\mu + q)^2$ and $(q + W)^2$ allowed. The larger $(\mu + q)^2$ and $(q + W)^2$ regions are most important and here the propagators go just as $1/(\mu + q)^2$ and $1/(q + W)^2$; thus the diagrams would be of relatively equal amplitude except for the factor of m_μ suppressing the muon pole. Therefore the ratio of $\sigma(m_\mu = 0)$ to $\sigma(m_\mu \neq 0)$ approaches 1. By similar arguments, one expects the ratio of W_1 cross sections to W_0 cross sections to approach 4. For high energies the dynamics are similar except for the factor of m_μ in the W_0 case; thus W_1 production has two equal diagrams or a relative cross section of 4, and W_0 production has one diagram or a relative cross section of 1.

κ Dependence

In W_1 production, diagram 3(a) dominates for all values of M_1. Since this diagram has no κ dependence (the W_1 does not interact electromagnetically in this diagram), the over-all κ dependence

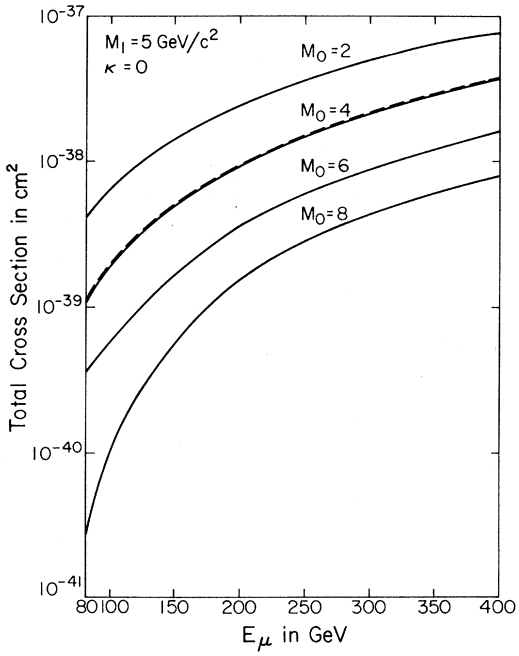

FIG. 11. W_0 (solid lines) and W_1 (dashed line) total production cross sections (per proton) by muons on iron vs muon energy. Here $M_1 = 5$ GeV/c^2, $M_0 = 2$, 4, 6, and 8 GeV/c^2, and $\kappa = 0$. For $M_0 = M_1$, W_0 production is approximately equal to W_1 production, and for $M_0 < M_1$, W_0 production exceeds W_1 production.

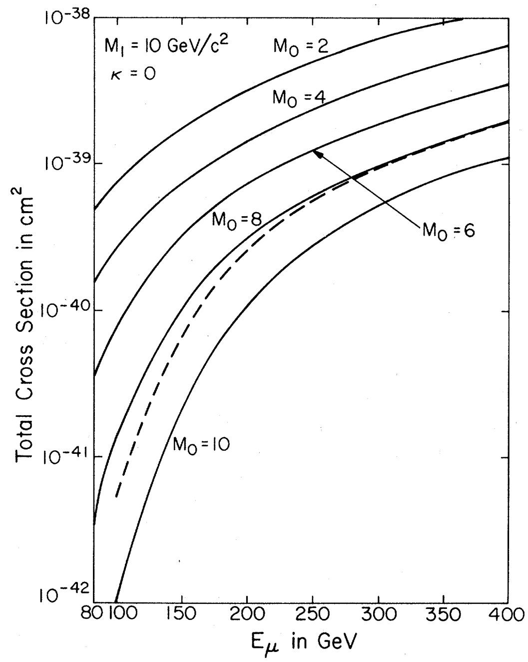

FIG. 12. Same as Fig. 11, but with $M_1 = 10$ GeV/c^2 and $M_0 = 2$, 4, 6, 8, and 10 GeV/c^2.

is very weak; the total cross sections increase with κ and between $\kappa = 0$ and $\kappa = \pm 1$ the difference is at most 20%. Since in W_0 production the diagram with the W propagator (and electromagnetic vertex) can dominate, one would expect more severe κ dependence. That is exactly the case as is apparent in Table VIII; the muon mass is zero, and the matrix element depends largely upon τ $(= 1 - \kappa)$. For $\kappa = 1$ and zero muon mass the cross sections fall drastically (by a factor of ≈ 100) since the quantity τ is zero. As κ decreases to -1, the cross sections increase up to a factor of 10. The difference (i.e., decrease with increasing κ vs increase with increasing κ in W_1 production) between this and the W_1 case presumably is a result of the different ways in which W_1's and W_0's couple electromagnetically. When nonzero muon mass is assumed, the drastic fall for $\kappa = 1$ is softened since the muon pole contributes, although the κ dependence is still strong unless it is a region where the muon pole dominates (M_1 greater than $\approx 4M_0$). In these regions the κ dependence is minimal. Figure 10 illustrates the difference in κ dependence between $M_1 = 15$ GeV/c^2 and $M_0 = 2$ GeV/c^2, where the muon pole dominates, and $M_1 = 15$ GeV/c^2 and $M_0 = 8$ GeV/c^2, where the muon pole is negligible. Interestingly, in the regions where the muon-propagator diagram dominates, the κ dependence of the coherent process is such that cross sections are bigger for $\kappa = \pm 1$ than for $\kappa = 0$, but, because of the κ dependence of the incoherent processes, the total κ dependence still decreases with increasing κ. This same effect occurs in muon-induced W_1 production (where the two diagrams are equally important). The effect apparently is interference between the two diagrams when their sizes are relatively the same.

In neutrino-induced W_0 production the effect of nonzero muon mass is only important when M_1 is greater than $\approx 4M_0$ or when κ is near 1. In these cases the muon-propagator diagram tends to be extremely important, making differences in total cross sections of factors of 10–1000. Elsewhere, the effect of nonzero muon mass is not important.

Incident Muons

The controversy over the muon mass is not crucial in the case of a muon beam. The first-order Feynman diagrams are illustrated in Figs. 3(c) and 3(d). The muon pole is damped just as in the neutrino case by a factor of m_μ, but in addition the denominator in the muon propagator cannot get very small. That denominator is

$$(\nu + W)^2 - m_\mu{}^2 = M_0{}^2 - m_\mu{}^2 + 2(\nu \cdot W). \tag{19}$$

If $(\nu \cdot W)$ is evaluated in the ν-W_0 center-of-mass frame, it is clear that $(\nu \cdot W)$ must be positive. The denominator can get no smaller than $M_0^2 - m_\mu^2$ and the advantage that the muon-propagator diagram had is lost. So with a muon beam the assumption of zero muon mass is a good one. Eventually, however, for M_1 much greater than $4M_0$ the phenomenon that occurred in the case of incident neutrinos should appear and the muon mass will again not be negligible. For reasonable ratios of M_1 to M_0 the assumption of zero muon mass is a good one.

In W_1 production with muons, the difficulty with the muon propagator reoccurs and W_1-production cross sections with muons are smaller than production with neutrinos by a factor of 100,[9] and are severely dependent upon κ, since diagram 3(c) does not dominate.

The only change that is necessary in order to calculate cross sections with a muon beam is the spin averaging. So to obtain muon-produced W_0 cross sections, it is only necessary to divide by 2 the results of neutrino-produced W_0 cross sections with zero mass. This factor of $\frac{1}{2}$ may be a bit generous, since the most energetic muons produced from π or K decay are right-handed for μ^-'s and left-handed for μ^+'s, which is the opposite helicity which is required to interact weakly. For consistency with other calculations, we present these calculations simply with the factor of $\frac{1}{2}$ for spin averaging.

Figures 11 and 12 show the W_0 total cross sections per proton on iron for several W_0 masses as a function of muon beam energy, for W_1 masses of 5 and 10 GeV/c^2, compared to the total cross sections for W_1 production.[9] The W_1-production cross sections and the W_0-production cross sections with M_0 set equal to M_1 are about equal for all energies. As M_0 decreases, W_0 production exceeds W_1 production. Both processes are extremely κ-dependent, the difference being that the W_1 cross sections are larger for $\kappa=\pm1$ than for $\kappa=0$, whereas the W_0 cross sections again decrease with κ. The κ behavior in W_1 production is presumably due to the interference of the two relatively equal diagrams. The κ behavior in the W_0 case is presumably due to the way in which the W_0 couples electromagnetically, since there is no diagram of equal size to interfere with. When divided by 2 the numbers in Tables I–IV for zero muon mass give the corresponding W_0-production cross sections for a muon beam.

IV. DIFFERENTIAL DISTRIBUTIONS

Monte Carlo Technique

It is possible to find the differential cross section as a function of any variables that can be expressed in terms of the variables $|t|$, $|\alpha|$, ξ, and ϕ_+ (for the definition of ξ and ϕ_+, see the Appendix) by transforming the variables and multiplying

$$\frac{d\sigma}{d|t|d|\alpha|d\xi\, d\phi_+}$$

by the appropriate Jacobian. In order to obtain differential cross sections of fewer variables, integrations can be performed. In general, the Jacobians and integrations involved are rather horrendous. Therefore, the problem of calculating differential distributions lends itself nicely to Monte Carlo techniques.

The Monte Carlo technique as employed here is stated simply as follows. First the variables $|t|$, $|\alpha|$, ξ, and ϕ_+ are transformed to τ, $|\alpha|$, θ_+, and ϕ_+, where

$$\tau=\exp[-b(|t|-|t_{\min}|)] \tag{20}$$

and

$$\cos\theta_+=\xi/|\alpha|\Gamma\,. \tag{21}$$

This is done in order to smooth out the behavior in $|t|$ and ξ. The constant b is chosen so that τ approximately follows $d\sigma/d|t|$; b is taken to be 4 GeV^{-2} in the incoherent case and 40 GeV^{-2} in the coherent case. The transformation is simply

$$f'(\tau,\,|\alpha|,\,\theta_+,\,\phi_+)=f(|t|,\,|\alpha|,\,\xi,\,\phi_+)\frac{\partial(|t|,\,|\alpha|,\,\xi,\,\phi_+)}{\partial(\tau,\,|\alpha|,\,\theta_+,\,\phi_+)} \tag{22}$$

and reduces to

$$f'(\tau,\,|\alpha|,\,\theta_+,\,\phi_+)=f(|t|,\,|\alpha|,\,\xi,\,\phi_+)\frac{|\alpha|\Gamma\sin\theta_+}{b\tau}, \tag{23}$$

where $f(|t|,\,|\alpha|,\,\xi,\,\phi_+)$ is given in the Appendix. Events are then chosen uniformly and randomly in the four-space of τ, $|\alpha|$, θ_+, and ϕ_+. The events are binned according to the variables of interest and weighted by $f'(\tau,\,|\alpha|,\,\theta_+,\,\phi_+)$. It is an easy matter to calculate the statistical error for any bin. It is simply

$$\sigma_{\text{bin}}=\left(\sum_{i=1}^{n}f_i'^2\right)^{1/2}, \tag{24}$$

where f_i' is the weight of the ith event in the bin. If the weights are equal, then the error is just

$$\sigma_{\text{bin}}=\sqrt{n}\,f'\,. \tag{25}$$

In order to check the above procedure, all the bins can be added together and the sum should just be the cross section within the statistical error. This serves both as a check on the numerical integrations and on the Monte Carlo procedure. For all the distributions presented here such checks have been made and all agreed within

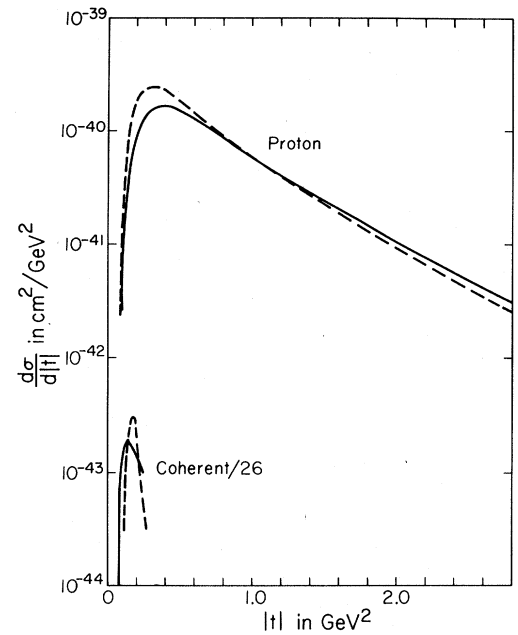

FIG. 13. $d\sigma/d|t|$ for W_0 production by neutrinos with $M_1 = M_0 = 5$ GeV/c^2 (solid lines) and $d\sigma/d|t|$ (not normalized) for W_1 production by muons with $M_1 = 5$ GeV/c^2 (dashed lines). Here $E_{\text{incident}} = 50$ GeV and $\kappa = 0$. In both processes the W-propagator diagram is important.

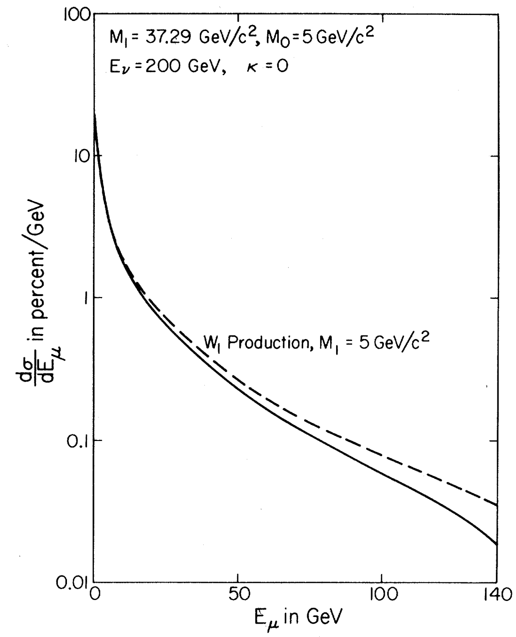

FIG. 15. $d\sigma/dE_\mu$ for W_0 production on iron by neutrinos with $M_1 = 37.29$ GeV/c^2 and $M_0 = 5$ GeV/c^2 (solid line) and $d\sigma/dE_\mu$ for W_1 production on iron with neutrinos for $M_1 = 5$ GeV/c^2 vs muon energy (normalized to 100%). Here $E_\nu = 200$ GeV and $\kappa = 0$. Both processes are dominated by the muon pole and are characterized by a spike of low-energy muons.

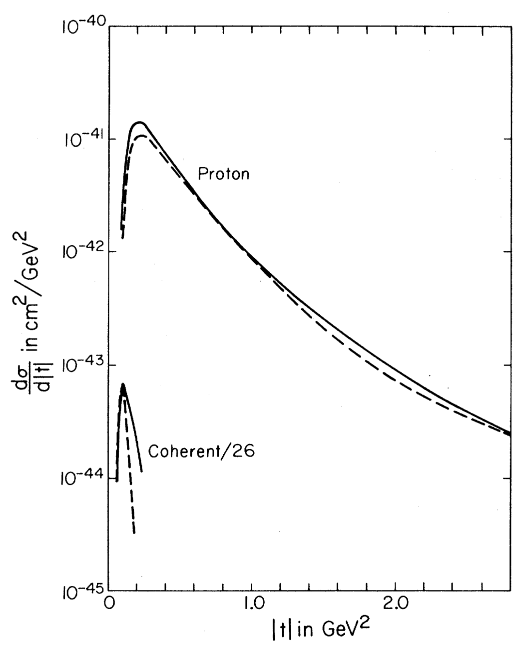

FIG. 14. $d\sigma/d|t|$ for W_0 production by neutrinos with $M_1 = 37.29$ GeV/c^2 and $M_0 = 5$ GeV/c^2 (solid lines) and $d\sigma/d|t|$ (not normalized) for W_1 production by neutrinos with $M_1 = 5$ GeV/c^2 (dashed lines). Here $E_\nu = 50$ GeV and $\kappa = 0$. In both processes the muon-propagator diagram is dominant. $d\sigma/d|t|$ falls faster here than when the W-propagator diagram dominates.

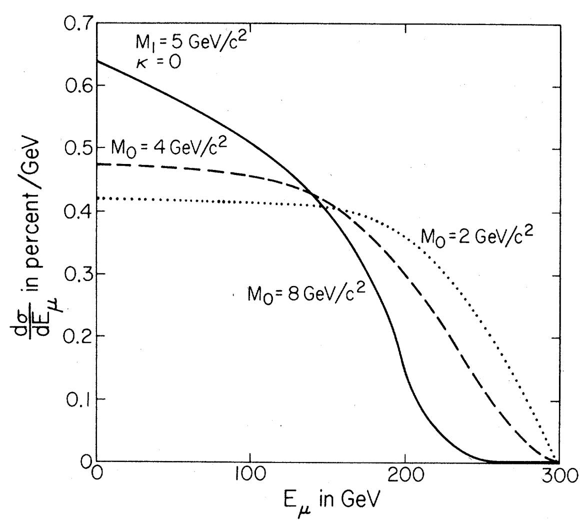

FIG. 16. $d\sigma/dE_\mu$ for W_0 production by neutrinos on iron for $M_1 = 5$ GeV/c^2, $E_\nu = 200$ GeV, $\kappa = 0$, and $M_0 = 2$ (dotted line), 4 (dashed line), and 8 GeV/c^2 (solid line) vs muon energy (normalized to 100%). Here the W pole dominates and is characterized by an almost constant distribution which approaches a linear decrease as M_0 increases (or E_ν decreases).

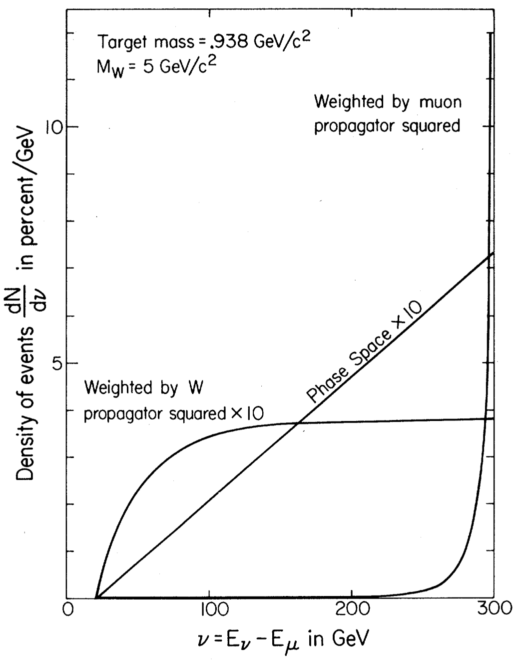

FIG. 17. Phase-space distribution of events as a function of energy transfer ν ($=E_\nu - E_\mu$) weighted by a constant factor of 10, by 10 times the W propagator squared, and by the muon propagator squared. Here a 300-GeV neutrino is incident upon a nucleon target producing a 5-GeV/c^2 W. Pure phase space is characterized by a linear rise, phase space weighted by the muon propagator squared by a spike for large ν's, and phase space weighted by the W propagator squared by an almost constant distribution of events.

the statistical and numerical integration errors involved. For each distribution 5000 events have been generated. To generate a set of three distributions (neutron, proton, and coherent), approximately 90 sec of compute time was required on an IBM 370/155.

Neutrinos: $d\sigma/d|t|$

The differential cross section as a function of $|t|$ has two sets of distinct shapes. For the incoherent process, when the W-propagator diagram dominates, the shape is characterized by a sharp rise and an exponential decay, as shown in Fig. 13. The shape is almost identical to that for muon-induced W_1 production, where the equivalent of diagram 3(b) is also important; this similarity is also illustrated in Fig. 13.[9] The shape of $d\sigma/d|t|$ goes as $e^{-b|t|}$, where b is between 2 and 5 GeV^{-2} and increases as the process is further above threshold. When diagram 3(b) dominates, the coherent process is characterized by a fast rise and fall. The spikelike shape is caused by the sharp nuclear form factor. Again, the shape is nearly identical to the shape for muon-induced W_1 production, the difference being in the form factor used (for the W_1 results, the Fermi charge distribution was assumed in order to calculate the form factor).

When the muon pole is most important (i.e., for M_1 greater than $\approx 4M_0$ or $\kappa = 1$), the corresponding curves are characterized by steeper falls and are nearly identical to the corresponding curves for neutrino-induced W_1 production. Here the b's for the incoherent case range between 4 and 7 GeV^{-2}. Figure 14 illustrates the similarity of the $d\sigma/d|t|$ curves for W_0 and W_1 production with neutrinos when the diagram with the muon propagator dominates.[9]

When the W pole is important (W_1 production by muons or W_0 production when $M_1 < 4M_0$ and $\kappa \neq 1$), $d\sigma/d|t|$ for W_1 production has a steeper fall than for W_0 production. This is reasonable since in W_1 production by muons the W-pole and muon-pole diagrams are relatively equal, whereas in W_0 production the muon pole (characterized by steeper falls in $d\sigma/d|t|$) is severely suppressed.

The Energy Distribution of the μ and W

By energy conservation,

$$E_\nu = E_\mu + E_W + \Delta E_{\text{target}}\,, \tag{26}$$

where ΔE_{target} is just E_q in the previous notation, and can be calculated as follows:

$$p_0 \cdot q = mE_q\,, \tag{27}$$

$$p_0 = \tfrac{1}{2}(P - q)\,, \quad P = p + p_0 \tag{28}$$

$$p_0 \cdot q = \tfrac{1}{2} q \cdot (P - q) = -\tfrac{1}{2} q^2\,, \tag{29}$$

and finally

$$E_q = |t|/2m\,. \tag{30}$$

For all the processes involved, $|t|$ is small (<10 GeV^2, since $d\sigma/d|t|$ falls rapidly). Therefore, for all practical purposes ΔE_{target} is zero and the beam energy is shared exclusively between the muon and the W_0, so $d\sigma/dE_W$ can be obtained from $d\sigma/dE_\mu$ by transforming the energy scale, $E_W \to E_\nu - E_\mu$.

In the case of W_1 production, the W_1 takes away almost all the beam energy. A plot of $d\sigma/dE_\mu$ for W_1 production is shown in Fig. 15.[12] In W_0 production there are two separate cases, as usual. When the W-propagator diagram dominates (for $M_1 < 4M_0$ and $\kappa \neq 1$), the distribution $d\sigma/dE_\mu$ is almost flat, as shown in Fig. 16. When muon-propagator diagram dominates (for $M_1 > 4M_0$ or κ near 1), the distribution is strongly peaked for low-energy muons. This case is almost identical to W_1 production, as also shown in Fig. 15.

The explanation for all this is simple. Figure 17 shows a plot of only phase space (i.e., $d^3W\, d^3\mu\, d^3p/E_W E_\mu E_p$) for an incident neutrino energy of 300

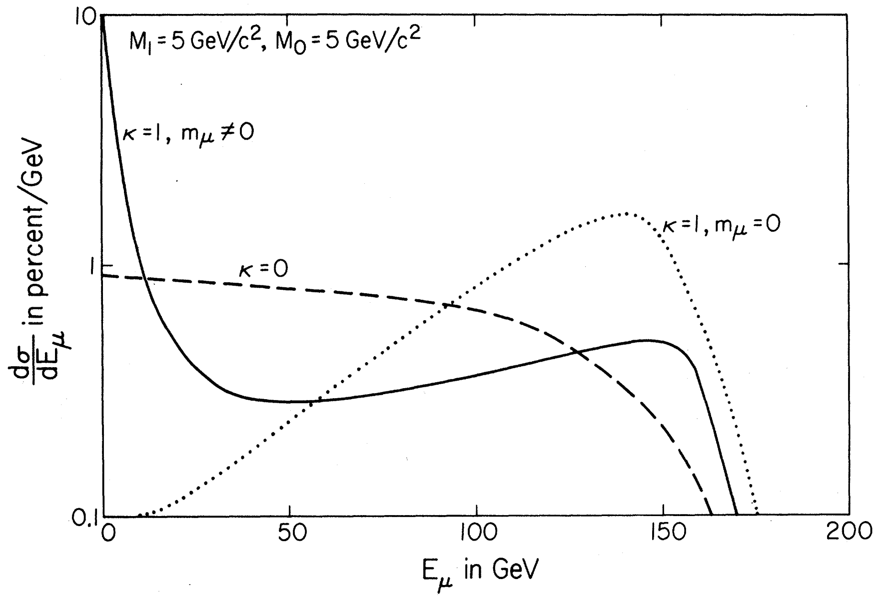

FIG. 18. $d\sigma/dE_\mu$ (normalized to 100%) for W_0 production by neutrinos on iron with $M_1 = M_0 = 5$ GeV/c^2 and $E_\nu = 200$ GeV for $m_\mu \neq 0$ and $\kappa = 1$ (solid line), $m_\mu \neq 0$ and $\kappa = 0$ (dashed line), and $m_\mu = 0$ and $\kappa = 1$ (dotted line). For $\kappa = 0$ the W pole dominates and the distribution is nearly constant; when the W pole dominates and $\kappa = 1$ ($m_\mu = 0$, $\kappa = 1$), $d\sigma/dE_\mu$ rises with E_μ. When $\kappa = 1$ and $m_\mu \neq 0$, $d\sigma/dE_\mu$ is characterized by a superposition of a low-energy spike (from the muon pole) and a slight rise with E_μ (from the W pole).

GeV, a nucleon target, and a 5-GeV/c^2 W. As a function of energy transfer ν ($=E_\nu - E_\mu$), phase space increases almost exactly linearly. Also shown in Fig. 17 is phase space weighted by the muon propagator squared and by the W propagator squared. When weighted by the muon propagator squared most of the events occur with large ν's (i.e., small muon energy). When weighted by the W propagator squared the events are spread almost equally for all the kinematically allowed ν's. This is precisely how $d\sigma/dE_W$ behaves. When the μ-propagator diagram dominates (W_1 production, and W_0 production for $M_1 > 4M_0$ and κ near 1), the W takes away most of the energy, and when the W-propagator diagram dominates, the distribution $d\sigma/dE_\mu$ (or $d\sigma/dE_W$) is constant.

In W_1 production, the muon-propagator diagram dominates and the W_1 takes away practically all the energy. In the neutrino-target center-of-mass frame the W_1 is going forward (in the direction of the neutrino) and the muon and target are going backwards. All the particles must be nearly collinear for the maximum W_1 energy configuration. In this configuration, spin along the neutrino direction must be conserved, since no orbital angular momentum is possible along this axis. The neutrino and muon "want" to be left-handed and the only way for this to be is if the W_1 spins left-handedly (assuming the target does not flip spin, which is reasonable since the process proceeds mainly by coupling to the charge, not to the magnetic moment, and in the coherent case the target spin is assumed to be zero). This explains the strong tendency for the W_1 to be left-handed and take away most of the beam energy in W_1 production.[13]

When M_1 is less than $4M_0$ and $\kappa \neq 1$, $d\sigma/dE_\mu$ is almost flat, and as the process gets closer to threshold (i.e., as M_0 increases or E_ν decreases), the muon energy spectrum begins to fall off linearly, as shown in Fig. 16. Varying κ does not affect the muon spectrum except near $\kappa = 1$. Here two things happen: If the muon mass is set equal to zero, the low-energy muons disappear completely and $d\sigma/dE_\mu$ rises with energy. For nonzero muon mass, when κ is nearly 1, the muon pole becomes important and the net result is a spike for low-energy muons and a gentle rise in $d\sigma/dE_\mu$ with increasing muon energy. This is all shown in Fig. 18.

When the muon pole dominates, there tends to be a spike for low-energy muons. The sharpness of this spike decreases slightly as the process gets closer to threshold. The muon spectrum is almost independent of κ when the muon pole dominates.

For fixed M_0, as M_1 increases, $d\sigma/dE_\mu$ changes from a flat spectrum to an almost pure phase-space spectrum (linearly decreasing), and then to a low-energy spike. This corresponds to moving from dominance by the W-propagator diagram to dominance by the muon-propagator diagram.

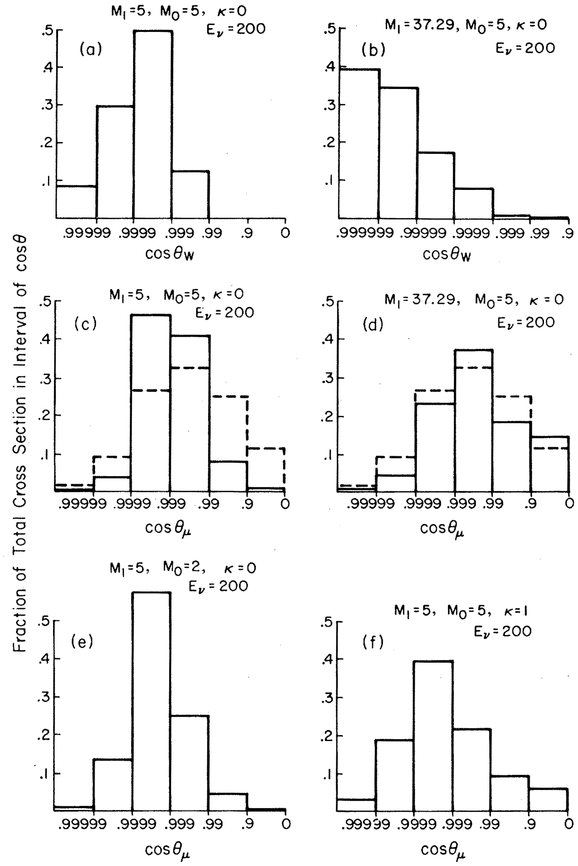

FIG. 19. Histograms of $d\sigma/d\cos\theta_{W_0}$ for W_0 production [19(a) and 19(b)] and of $d\sigma/d\cos\theta_\mu$ in W_1 (dashed lines) and W_0 (solid lines) production by neutrinos on iron. In W_1 production, $M_1=5$ GeV$/c^2$, $E_\nu=200$ GeV, and $\kappa=0$. In W_0 production when the muon pole dominates [19(b) and 19(d)], the W_0 angles are very small (as are the W_1 angles in W_1 production) and the muon angular distributions are similar to those for W_1 production. When the W pole dominates [19(a), 19(c), 19(e), and 19(f)], the W_0 angles are larger (than the W_1 angles) and the muon angles smaller than in W_1 production.

The W_0 Angle

In W_1 production with neutrinos the process was characterized by small-angle muons and extremely small-angle W_1's in the lab system. The situation in W_0 production is similar. The W_0 angles (in the lab system) are very small. Figures 19(a) and 19(b) compare the W_0 angular distribution as a function of $\log(1-\cos\theta_{W_0})$ for two cases; Fig. 19(a) shows the distribution when the W-propagator diagram dominates, and Fig. 19(b) when the muon-propagator diagram dominates. The W_0 angles are much smaller when the muon pole dominates, which is reasonable, because in this case the W_0 comes out essentially forward in the neutrino-target center-of-mass system. The W_0 angles when the muon pole dominates are the same as the W_1 angles in W_1 production, while the W_0 angles when the W-propagator diagram dominates tend to be larger than those in W_1 production.

The Muon Angle

The muon angle tends to be smaller for W_0 production than for W_1 production if the W-propagator diagram is most important. When the muon-pole dominates, the angular distribution tends to be identical to that for W_1 production. Figures 19(c) and 19(d) illustrate this.[12] That the muon angles should be smaller when the W-propagator diagram dominates is expected, since in this case the muons tend to be more energetic (than in W_1 production) and hence more forward in the neutrino-target center-of-mass frame.

When the process is further above threshold the angles become smaller, as is evident by comparing Fig. 19(c) with Fig. 19(e). For fixed M_0, as M_1 increases, the muon angle tends to increase until the muon pole becomes important, and then the distribution remains constant and almost identical to that for W_1 production with W_1 mass equal to the W_0 mass (i.e., the same kinematics).

For κ not near 1, the muon angular distribution is essentially independent of κ. When κ is near 1 and M_1 is not greater than $\approx 4M_0$, the fractions of muons with small angles and large angles increase with respect to the same distribution for $\kappa=0$, as can be seen by comparing Figs. 19(c) and 19(f). The reason for this is simple. It was mentioned previously that the muon energy distribution under similar circumstances increased in the number of low- and high-energy muons, the increase in high-energy muons being due to the W-pole propagator diagram and the increase in low-energy muons being due to the muon pole. The low-energy muons are characterized by large angles and the high-energy muons by small angles, so the changes in $d\sigma/dE_\mu$ and $d\sigma/d\cos\theta_\mu$ are a result of the same thing.

Incident Muons

The distributions for incident muons have the same characteristics as the distributions for incident neutrinos when the W-propagator diagram dominates. That is, briefly, $d\sigma/d|t|$ falls roughly as $e^{-b|t|}$ with b's of 2–5 GeV^{-2} (see Fig. 13). The shape of $d\sigma/dE_W$ is nearly flat, with the low-energy end tapering off as M_0 increases and approaching a straight linear increase (pure phase space) as M_1 goes to infinity. When $\kappa=1$, $d\sigma/dE_W$ tends to decrease linearly, as shown in Fig. 18 (the abscissa should be transformed to E_W), with few high-energy W_0's. The W_0 angular distributions are not

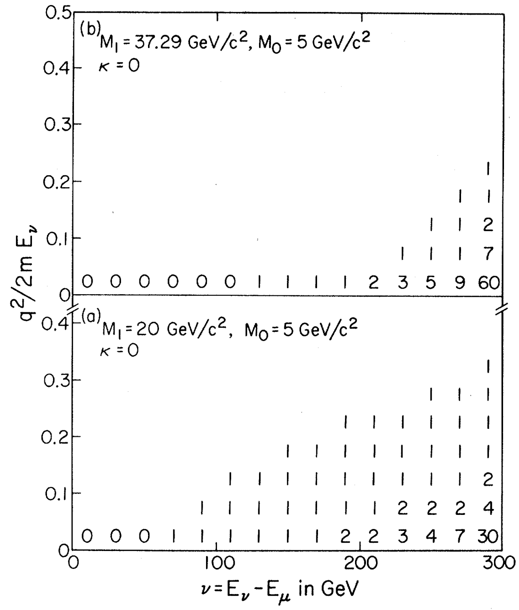

FIG. 20. q^2-ν distribution of 100 events of W_0 production by neutrinos on iron for $M_0 = 5$ GeV/c^2, $E_\nu = 300$ GeV, $\kappa = 0$, and $M_1 = 20$ and 37.29 GeV/c^2. As the ratio of M_1 to M_0 increases, the muon pole dominates more strongly and the events tend to cluster in a spike for large ν and small q^2.

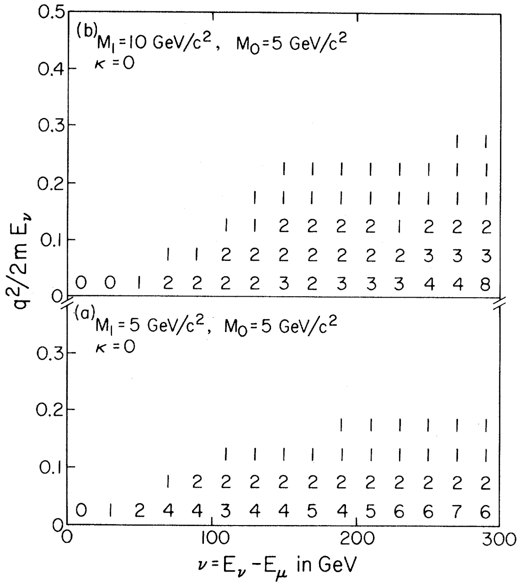

FIG. 21. q^2-ν distribution of 100 events of W_0 production by neutrinos on iron for $M_0 = 5$ GeV/c^2, $E_\nu = 300$ GeV, $\kappa = 0$, and $M_1 = 5$ [21(a)] and 10 GeV/c^2 [21(b)]. Here the W pole dominates and, as M_1 increases, the even distribution of events in a thin rectangle moves toward larger ν's and spreads upward in q^2.

as sharply peaked in small angles as in W_1 production. The neutrino angular distributions shift toward larger neutrino angles with increasing W_1 or W_0 mass or decreasing energy. When κ is near 1, the fraction of neutrinos at small (and large) angles increases with respect to the distributions for $\kappa = 0$ or $\kappa = -1$.

q^2 vs ν

In neutrino inelastic scattering a particularly useful parametrization of events is in terms of momentum transfer squared,

$$q^2 = |(\nu - \mu)^2| = |(q + W)^2| , \tag{31}$$

and energy transfer,

$$\nu = E_\nu - E_\mu . \tag{32}$$

q^2 has a range of 0–$2m\nu$ ($q^2 = 2m\nu$ is the quasielastic limit), where m is the mass of the target, and ν ranges from zero to almost beam energy. This is identical to the formalism used in inelastic electron scattering.

In W_1 production with neutrinos, the distribution of events in $q^2/(2m_p E_\nu)$ [14] and ν is concentrated in the lower right-hand corner [i.e., large ν and small $q^2/(2mE_\nu)$].[15] The distribution in ν is just a restatement of the earlier result that the W_1 carried away all the beam energy (large energy transfer). On the q^2-ν plot, lines of constant muon angle are straight lines extending from $q^2 = 0$ and $\nu_{\max}$, zero angle being along the ν axis and maximum angle parallel to the q^2 axis. The concentration of events with small q^2 and large ν yields no information about angle, since in that corner all possible muon angles are lumped together.

In W_0 production with neutrinos, there are two signatures.[14] First, when the muon-propagator diagram dominates, the signature is just like the signature in W_1 production and this is illustrated for W_0 production in Figs. 20(a) and 20(b). When the W-propagator diagram dominates, the signature is a nearly constant distribution of events in a thin rectangle (thin in the q^2 dimension and extending along the full ν axis), as shown in Figs. 21(a) and 21(b). The thin rectangle means that the muon or W_0 energy spectrum is flat and that the muon angle is characteristically small (all the events lie below a line of constant small angle). These results are consistent with the previous distributions in energy and angle.

In the regions where the muon pole dominates, when the process is closer to threshold, the spike becomes slightly less distinct, spreading out very slowly in both directions. When the muon pole dominates, the distribution is practically independent of M_1 and κ. When the W-propagator diagram dominates, as M_1 increases, the distribution of events spreads out rapidly in q^2 and approaches a linear rise in ν (pure phase space); this is easily

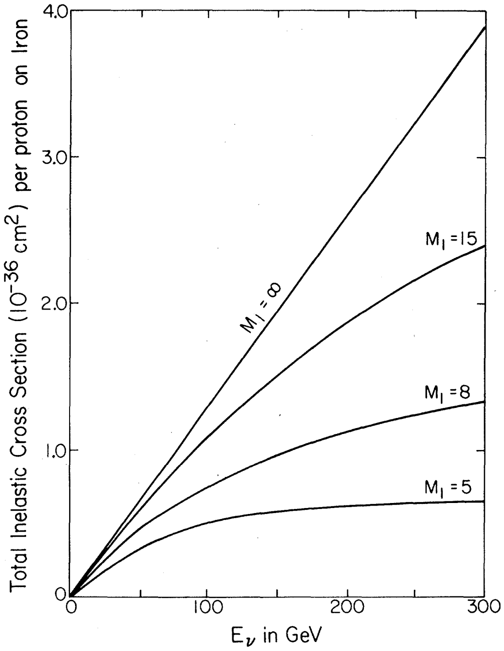

FIG. 22. Total inelastic neutrino cross section (per proton) on iron vs neutrino energy, assuming the model detailed in the text for W_1 masses of 5, 8, and 15 GeV/c^2.

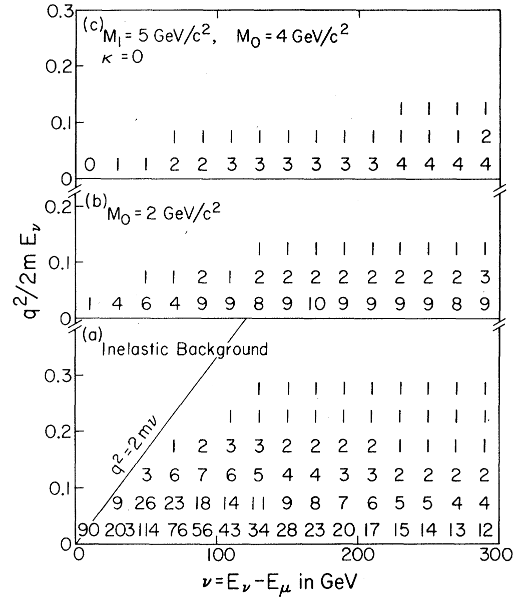

FIG. 23. q^2-ν distribution of 1000 inelastic neutrino events [23(a)], W_0-production events with $M_0=2$ GeV/c^2 normalized relative to the inelastic events [23(b)], and W_0-production events with $M_0=4$ GeV/c^2 also normalized relative to the inelastic events [23(c)] for $M_1=5$ GeV/c^2, $E_\nu=300$ GeV, and $\kappa=0$. The thin-rectangle signature is intelligible for small W_1 and W_0 masses ($\lesssim 5$ GeV/c^2).

predicted since the W propagator goes as

$$-1/(q^2+M_1^2), \tag{33}$$

and as M_1 increases, the propagator is more like $-1/M_1^2$ than $-1/q^2$ and therefore does not suppress large q^2's. Eventually, when M_1 is large enough, the muon pole dominates and most of the events lie in a narrow spike. Figures 21(a), 21(b), 20(a), and 20(b) show such a progression from W-pole dominance to muon-pole dominance.

When diagram 3(b) dominates, as the process moves closer to threshold, the events spread upward in the q^2 direction and move toward larger ν's. Unless κ is near 1 here, κ has little effect on the distribution in q^2 and ν. When κ is near 1 and M_1 is still less than $4M_0$, the distribution tends to be a superposition of a spike on a thin rectangle.[16]

The usefulness of the q^2-ν formalism is that it offers possible help in detecting the existence of a W_1 or a W_0 without actually detecting the particle itself. The W_1 signature is clear. It would appear as an energy-dependent spike on top of a background of neutrino inelastic scattering off nucleons. To assess the merit of a signature, it is necessary to estimate what the neutrino inelastic background might look like. At present neutrino beam energies, the neutrino inelastic cross section seems to rise linearly with beam energy at the rate of[17]

$$\sigma_{\text{inel}}(\text{per nucleon}) = 0.6\times10^{-38}\times E_\nu \text{ cm}^2. \tag{34}$$

The existence of a W boson would force this linear rise to turn over.

The differential inelastic cross section can be written as[18]

$$\frac{d^2\sigma}{dq^2 d\nu} = \frac{E_\nu-\nu}{E_\nu}\frac{G^2}{2\pi}\left\{\cos^2(\tfrac{1}{2}\theta)\left[W_2(q^2,\nu)+2\tan^2(\tfrac{1}{2}\theta)\left(W_1(q^2,\nu)-\frac{2E_\nu-\nu}{2m}W_3(q^2,\nu)\right)\right]\right\}, \tag{35}$$

where E_ν is the neutrino beam energy in the lab, m is the target mass, and θ is the muon lab angle. This formalism is identical to that for electron inelastic scattering, except for the addition of W_3 and the lack of a $1/q^4$ photon-propagator factor.

For a definite model for comparison, we will assume that Eq. (35) needs only to be modified by a W propagator squared, and that W_1 and W_2 exhibit scale invariance (i.e., are a function only of $x=q^2/2m\nu$), or, more precisely, that

$$\nu W_2 = F_2(x), \tag{36}$$

$$MW_1 = F_1(x), \tag{37}$$

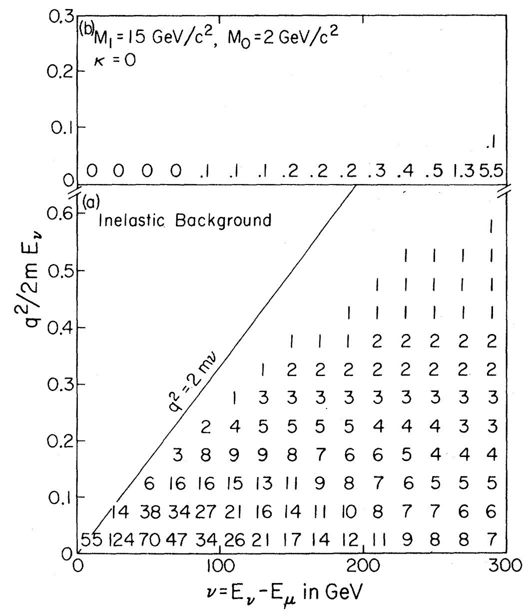

FIG. 24. q^2-ν distribution of 1000 neutrino inelastic events [24(a)] and W_0-production events with $M_0=2$ GeV/c^2 normalized relative to the inelastic background [24(b)] for $M_1=15$ GeV/c^2, $E_\nu=300$ GeV, and $\kappa=0$. The spike signature is intelligible for large values of W_1 mass and small values of W_0 mass.

and that $W_3=0$. Further, we suppose that the Callan-Gross relation[19]

$$F_2(x)=2F_1(x)x \tag{38}$$

holds here. Then we set

$$F_2(x)=F_2^{ep}(x)\,, \tag{39}$$

where $F_2^{ep}(x)$ are the SLAC data for F_2 in electron-proton inelastic scattering.[20] The cross section is normalized so that for $M_1=\infty$ the total inelastic cross section increases as $0.6\times E_\nu\times 10^{-38}$ cm^2.

Figure 22 shows the turnover of total inelastic cross section for several values of M_1 and this model. Figures 23(a) and 24(a) show the q^2-ν distribution of 1000 events for $M_1=5$ and 15 GeV/c^2 with beam energy of 300 GeV using this model. The events tend to be not as restricted in q^2 as W_0 and W_1 production events and tend to be more concentrated toward small values of ν.

Figures 23(b) and 23(c) show, respectively, the q^2-ν distributions of W_0 events for $M_1=5$ GeV/c^2, $E_\nu=300$ GeV, and M_0's of 2 and 4 GeV/c^2, normalized relative to the inelastic background shown in Fig. 23(a). For $M_0=2$ GeV/c^2 the signature is barely intelligible for large ν's. For $M_0=4$ GeV/c^2 the signature is almost indiscernible from the background. The thin-rectangle signature is intelligible for small values of M_0 and M_1 ($M_0, M_1 \lesssim 5$ GeV/c^2) using this model.

The spike signature, characteristic of the muon pole, offers better hope for detection since all the events tend to be concentrated in one corner of the q^2-ν plot and in this corner the inelastic background is not large. Figure 24(b) illustrates the distribution of events for $M_1=15$ GeV/c^2, $M_0=2$ GeV/c^2, and $E_\nu=300$ GeV, normalized relative to the inelastic background [Fig. 24(a)]. For relatively large W_1 masses (≥ 8 GeV/c^2) and small W_0 masses (≤ 4 GeV/c^2), the spike signature is intelligible.

In the case of a spikelike signature there is an additional problem – how to tell whether a W_0 or a W_1 was produced. If the cross sections are similar, and both are being produced, the spike should have a dual threshold behavior, since in this case the W_1 mass and W_0 mass would be very different. If the spike has only a single threshold behavior, identification is more difficult. For a spike with given size, a W_1 more massive than a W_0 is produced, so the severity of the energy dependence of the threshold is one means of identification. If a W_1 is produced, its effects upon neutrino inelastic cross sections should be predictable and measurable. A search for $\mu^-\mu^+$ pairs or high-energy γ rays (from $W_1\to W_0\gamma$) also serves to identify a W_1. A detailed examination of the hadronic debris might yield an estimate of the mass of the particle that is produced and from this it could be inferred whether a W_0 or W_1 was produced (for a spike with given size, the possible W_1 masses are much bigger than the possible W_0 masses). In any case, the identification process is not an easy task.

Incident Muons

For a muon beam, the significance of the q^2-ν plot is almost academic, because it is extremely difficult to measure either q^2 or ν since the outgoing particle is a neutrino. The signature is always a thin rectangle that spreads upward (in the q^2 direction) and approaches the phase-space distribution in the ν direction as M_1 increases. As the process gets closer to threshold, the distribution of events moves toward larger ν's, but never so much as to give a spike, as is characteristic of the muon pole.

V. CONCLUDING REMARKS

Except for large W_1 masses and small W_0 masses, W_1 production by neutrinos is a factor of 20–100 larger. When the ratio of W_1 mass to W_0 mass is greater than about 4 or κ is near 1, neglecting the muon mass is a very poor assumption. In these regions the finite muon mass greatly enhances the coherent cross section (by factors of up to 10 000).

With a muon beam, W_0 production is greater than W_1 production for fixed M_1 and M_0 less than or equal to M_1. Here the assumption of zero muon mass is a good one.

Each Feynman diagram has its characteristic shape. The muon-propagator diagram is characterized by low-energy outgoing muons, very small W_0 lab angles, rapidly falling differential cross section as a function of $|t|$, and a spike for large ν, with small q^2 on the q^2-ν plot. The W-propagator diagram is characterized by equal sharing of beam energy between the W_0 and muon, very small muon lab angles [smaller than for diagram 3(a)], small W_0 angles [but bigger than for diagram 3(a)], not as rapidly falling differential cross section as diagram 3(a), and a thin rectangle (narrow in q^2 and extending from $\nu_{\min}$ to $\nu_{\max}$) signature on the q^2-ν plot.

Unless the W_1 is very massive and the W_0 is much less massive, W_1 production exceeds W_0 production with neutrinos and the best way to produce a W_0 is through the decay of a W_1. The signature here is wide-angle high-energy γ rays (from $W_1 \to W_0\gamma$), and it is possible that the distribution of large-angle hadrons from the W_0 decay might provide an additional signature, depending upon what the hadronic distribution of the inelastic neutrino scattering background turns out to look like.

If there are two W's, both of small mass (≤ 5 GeV/c^2), the thin-rectangle signature on the q^2-ν plot in neutrino-induced production should serve to identify the W_0. If there are two W's and the W_1 is many times more massive than the W_0, then the W_0 will be easier to produce and its signature on the q^2-ν plot would be a nice spike. In this case, it is necessary to resolve whether a W_0, a W_1, or both, was or were produced.

A muon beam has the advantage of well-defined beam energy and the W_0 cross sections tend to be equal to or larger (unless $M_0 > M_1$) than corresponding W_1-production cross sections. The cross sections for a muon beam are smaller by a factor of $\frac{1}{2}$ (except in regions where the muon pole dominates in neutrino production) than for a neutrino beam and, because of the difficulty in measuring the outgoing neutrino's four-momentum, a q^2-ν plot is impossible to make. With incident muons, any W_0 search must concentrate strictly on decay products.

As mentioned earlier, it is possible to produce a W_0 in a variety of other ways. In these processes (e^-e^+ colliding beams, nucleon-nucleon collisions, etc.), the key to detection is an anomalous behavior in the distribution of wide-angle hadrons. None of the methods of production or detection offer an immediate, sure, and simple way to search for the possible existence of a W_0. Careful examination of data that are soon to be available from experiments at NAL seems to offer the best and most immediate hope of searching for a W_0.

Note added. Our results now agree with those done by Reiff.[21] He discovered a mistaken overall factor of $(M_0/M_1)^2$ in his calculations. This change affected some of his conclusions, but his conclusion concerning the assumption of zero muon mass remains unaffected.

ACKNOWLEDGMENTS

One of us (M.S.T.) would like to thank Jon Mathews for his help in checking the complex matrix element that is involved for nonzero muon mass by independently squaring it and comparing terms. We would also like to thank Piermaria Oddone and George Zweig for their helpful conversations.

APPENDIX

The procedures used to calculate the differential cross section $d^2\sigma/d|t|d|\alpha|$ for W_0 production with neutrinos are detailed in this Appendix. It is useful to define the following invariants:

$$y = 1/[(\mu+q)^2 - m_\mu^2], \tag{A1}$$

$$z = 1/[(W+q)^2 - M_1^2], \tag{A2}$$

$$\alpha = \nu \cdot q, \tag{A3}$$

$$t = q^2, \tag{A4}$$

$$x = -\alpha + \tfrac{1}{2}t, \tag{A5}$$

$$\beta = \frac{[(M_1^2 - M_0^2)/M_1^2]\kappa q^2 - 2/z}{q^2 + 2q\cdot W}, \tag{A6}$$

$$\tau = 1 - \kappa. \tag{A7}$$

The matrix element can be expressed as

$$W_\alpha O_{\alpha\beta} v_\beta, \tag{A8}$$

where $O_{\alpha\beta}$ is

$$\{-2y\mu_\beta l_\alpha + l_\beta[(z\tau - y)q_\alpha + (zq^2 - 1)W_\alpha/W^2] + \delta_{\alpha\beta}(y - z\tau)q\cdot l - y\epsilon_{\beta\alpha\lambda\eta}q_\lambda l_\eta - z\beta(q+W)\cdot l\,\delta_{\alpha\beta}\}e^2 g/M_1 q^2 \tag{A9}$$

and

$$l_\alpha = \bar{u}_\mu \gamma_\alpha (1-\gamma_5) u_\nu\,. \tag{A10}$$

The square of the matrix element is just

$$W_\alpha W^*_{\alpha'} O_{\alpha\beta} O^*_{\alpha'\beta'} v_\beta v^*_{\beta'}\,. \tag{A11}$$

The spin summations can be done simply by using the following identities:

$$\sum_{\mu,\nu\ \text{spins}} l_\alpha l_\beta^* = 8[\mu_\alpha \nu_\beta + \mu_\beta \nu_\alpha - \delta_{\alpha\beta}(\mu\cdot\nu) + i\epsilon_{\beta\alpha\xi\eta}\mu_\xi\nu_\eta] \tag{A12}$$

and

$$\frac{1}{2}\sum_{\text{spin}} v_\beta v_{\beta'}^*/m^2 = \Psi_2(t)P_\beta P_{\beta'} + \Psi_3(t)(q^2\delta_{\beta\beta'} - q_\beta q_{\beta'}), \tag{A13}$$

where $P=p_0+p$ and m is the target mass. $\Psi_2(t)$ and $\Psi_3(t)$ are related to the nucleon form factors as follows:

$$\Psi_2(t) = \frac{G_E{}^2 - (t/4m^2)G_M{}^2}{(1-t/4m^2)m^2} \tag{A14}$$

and

$$\Psi_3(t) = G_M{}^2/m^2 \tag{A15}$$

for a proton or neutron target. G_M and G_E are the usual SLAC dipole-fit form factors[4]

$$G_E^p = \left(\frac{1}{1-t/0.71}\right)^2, \tag{A16}$$

$$G_M^p = G_E^p(1+\kappa_p), \tag{A17}$$

$$G_E^n = 0, \tag{A18}$$

$$G_M^n = G_E^p \kappa_n . \tag{A19}$$

κ_p and κ_n are the anomalous magnetic moments of the proton and neutron, respectively. For the coherent process, $\Psi_3(t)$ is set equal to zero (i.e., the spin of the nucleus is neglected) and $\Psi_2(t)$ is taken to be the nuclear dipole form factor divided by the mass of the nucleus squared,

$$\Psi_2(t) = \frac{|F_0(q^2)|^2}{m^2} = \frac{1}{(1-\frac{1}{12}q^2a^2)^4 m^2}, \tag{A20}$$

where

$$a^2 = \tfrac{3}{5}(1.3\times 10^{-13}A^{1/3})^2\ \text{cm}^2 . \tag{A21}$$

The differential cross section summed over spin can now be written as

$$d\sigma = [\Psi_2(t)P_\beta P_{\beta'} + \Psi_3(t)(t\delta_{\beta\beta'} - q_\beta q_{\beta'})][S_0\delta_{\beta\beta'} + S_1 W_\beta W_{\beta'} + S_2(W_\beta \mu_{\beta'} + \mu_\beta W_{\beta'}) + S_3\mu_\beta\mu_{\beta'}]$$
$$\times \frac{m^2 e^4 g^2}{q^4 M_1{}^2}\, 8\, \frac{d^3\mu\, d^3p\, d^3W (2\pi)^4 \delta^4(\nu - q - W - \mu)}{2E_W 2E_\nu 2E_\mu 2m 2E_p (2\pi)^9} . \tag{A22}$$

The coefficients S_i contain all the terms in the expression

$$\tfrac{1}{8}O_{\alpha\beta}O^*_{\alpha'\beta'}W_\alpha W^*_{\alpha'} . \tag{A23}$$

Table V contains the coefficients S_i in terms of dot products, and Tables VI and VII contain the S_i in terms of t and constants; here

$$S_a = \sum_{b,c} y^b z^c S_{abc} + S_a(\beta) . \tag{A24}$$

The terms arising from the β term in Eq. (A9) are segregated since they involve a third denominator, $q^2+2q\cdot W$ (in addition to y and z). Here

$$S_a(\beta) = \sum_{b,c,d} y^b z^c \left(\frac{1}{q^2+2q\cdot W}\right)^d S_{abcd} . \tag{A25}$$

Following the procedures of Wu and Yang,[3] the phase-space volume element

$$\frac{d^3\mu\, d^3p\, d^3W}{E_\mu E_p E_W}\delta^4(\nu - W - q - \mu) \tag{A26}$$

is transformed to the μ-W_0 center-of-mass frame; Fig. 25 illustrates this coordinate system. The vector $\vec{\nu}$ is taken along the z axis, and in this frame $\vec{q}=\vec{\nu}$. The direction of $\vec{W}$ is specified by its polar angle θ_+ and azimuthal angle ϕ_+. The target momenta $\vec{p}_0$ and $\vec{p}$ are taken to lie in the xz plane. The outgoing target polar and azimuthal angles in the lab frame are θ_p and ϕ_p, respectively.

The phase-space volume element

TABLE V. The coefficients S_i in Eq. (A22) in terms of dot products.

S_3:	$y^2[8\nu\cdot W(q\cdot W+\mu\cdot W)+2q^2W^2+4W^2(\mu\cdot q-\mu\cdot\nu-\nu\cdot q)]+yz\{4(2\nu\cdot W-W^2)[(1+\kappa)q\cdot W+W^2-M_1{}^2]\}$ $+z^2\{2[(1+\kappa)q\cdot W+W^2-M_1{}^2]^2\}$
S_2:	$y^2[(q^2+2\mu\cdot q)(W^2-2\nu\cdot W)]+yz[\tau(2\nu\cdot W-W^2+q\cdot W)(q^2+2\mu\cdot q)+2(2\nu\cdot W-W^2)(2q\cdot W+W^2-M_1{}^2)]$ $+z^2\{[(1+\kappa)q\cdot W+W^2-M_1{}^2][\tau(2\mu\cdot q+q^2)+2q\cdot W+W^2-M_1{}^2]\}+\{z\beta[(z\tau-y)q\cdot W+zq^2-1]m_\mu{}^2-2yz\beta\nu\cdot W m_\mu{}^2\}$
S_1:	$yz[2\tau(q^2m_\mu{}^2-q^2\mu\cdot q-2\mu\cdot q^2)]+z^2[2\tau\mu\cdot q(q^2+2q\cdot W+W^2-M_1{}^2+\tau\mu\cdot q+\tau q^2)-\tau q^2(\tau\mu\cdot\nu+2\mu\cdot q)]$ $+\{2z\beta[(z\tau-y)q\cdot W+zq^2-1]m_\mu{}^2-2z\beta(z\tau-y)\nu\cdot q m_\mu{}^2+z^2\beta^2\mu\cdot\nu m_\mu{}^2\}$
S_0:	$y^2[W^2(2\mu\cdot q\,\nu\cdot q-q^2\mu\cdot\nu)-2\nu\cdot W(2q\cdot W\mu\cdot q-q^2\mu\cdot W)]+yz\{2(\nu\cdot W\mu\cdot q+\mu\cdot\nu q\cdot W-\mu\cdot W\nu\cdot q)[(-1-\kappa)q\cdot W-W^2+M_1{}^2]\}$ $+z^2\{-\mu\cdot\nu[(1+\kappa)q\cdot W+W^2-M_1{}^2]^2\}$

TABLE VI. The tensor S_{abc} defined in Eq. (A24). $\Delta=\tau(M_0^2-M_1^2+t)-2t$.

b	c	a: 0	1	2	3
−2	2		$\frac{1}{2}\tau^2$		
−1	1			$-\frac{1}{2}\tau^2$	
−1	2		$-\tau t$	$\frac{1}{2}\Delta\tau$	
0	−1	$\frac{1}{8}\tau^2$			
0	0	$-m_\mu{}^2\frac{1}{2}\kappa-\frac{1}{4}\tau\Delta-\frac{1}{8}\tau^2(m_\mu{}^2-M_1{}^2)$			$\frac{1}{2}\tau^2$
0	1	$-\frac{1}{2}m_\mu{}^2\Delta+\frac{1}{8}\Delta^2+\frac{1}{4}\tau\Delta(m_\mu{}^2-M_1{}^2)$	$\frac{1}{2}\tau^2 t$	$-\tau(m_\mu{}^2-\frac{1}{2}t)$	$-\tau\Delta$
0	2	$-\frac{1}{8}\Delta^2(m_\mu{}^2-M_1{}^2)$	$-\frac{1}{2}\tau^2 t\,(m_\mu{}^2-M_1{}^2+t)+\tau t^2$	$-\frac{1}{2}\Delta t$	$\frac{1}{2}\Delta^2$
1	−1	$-\frac{1}{2}m_\mu{}^2\kappa$			
1	0	$+\frac{1}{2}m_\mu{}^2[\kappa(M_0{}^2-M_1{}^2)-\Delta+t]$		$-m_\mu{}^2$	$2\tau m_\mu{}^2$
1	1	$+\frac{1}{2}m_\mu{}^2\Delta\,(M_0{}^2-M_1{}^2)$	$2\tau m_\mu{}^2 t$	$2tm_\mu{}^2$	$-2\Delta m_\mu{}^2$
2	0	$+\frac{1}{2}m_\mu{}^2 t\,(m_\mu{}^2-M_0{}^2)$			$2m_\mu{}^2(m_\mu{}^2-M_0{}^2)$

$$\frac{d^3\mu\, d^3W\, d^3p}{E_\mu E_W E_p}\delta^4(\nu-W-q-\mu) \tag{A27}$$

transforms to

$$\frac{d|t|d|\alpha|d\xi d\phi_+ d\phi_p}{4mE_\nu|\alpha|}, \tag{A28}$$

where ξ is defined by

$$\xi=|\alpha|\Gamma\cos\theta_+ \tag{A29}$$

and

$$\Gamma=\{[x+\tfrac{1}{2}(M_0{}^2-m_\mu{}^2)]^2-2M_0{}^2x\}^{1/2}/x. \tag{A30}$$

The differential cross section is now

$$d\sigma=[\Psi_2(t)P_\beta P_{\beta'}+\Psi_3(t)(t\delta_{\beta\beta'}-q_\beta q_{\beta'})][S_0\delta_{\beta\beta'}+S_1W_\beta W_{\beta'}+S_2(W_\beta\mu_{\beta'}+\mu_\beta W_{\beta'})+S_3\mu_\beta\mu_{\beta'}]$$
$$\times\frac{d|t|d|\alpha|d\xi d\phi_+ d\phi_p}{t^2|\alpha|}\frac{H}{(2\pi)^2}, \tag{A31}$$

TABLE VII. The tensor S_{abcd} defined in Eq. (A25). $c=-\kappa t(M_1{}^2-M_0{}^2)/M_1{}^2$.

b	c	d	$S(\beta)_{abcd}$, a: 1	2
−1	1	1	$2m_\mu{}^2\tau$	
−1	2	1	$m_\mu{}^2c\tau$	
0	−1	2	$-2m_\mu{}^2$	
0	0	1	$2m_\mu{}^2$	$-\tau m_\mu{}^2$
0	0	2	$2m_\mu{}^2(m_\mu{}^2-M_1{}^2)-2m_\mu{}^2c$	
0	1	1	$+m_\mu{}^2c+2\tau m_\mu{}^2t-4m_\mu{}^2t$	$-\frac{1}{2}cm_\mu{}^2\tau-2m_\mu{}^2t+\tau m_\mu{}^2(M_0{}^2-M_1{}^2+t)$
0	1	2	$2m_\mu{}^2c(m_\mu{}^2-M_1{}^2)-\frac{1}{2}c\,m_\mu{}^2$	
0	2	1	$\tau cm_\mu{}^2t-2cm_\mu{}^2t$	$-m_\mu{}^2ct+\frac{1}{2}cm_\mu{}^2\tau(M_0{}^2-M_1{}^2+t)$
0	2	2	$+\frac{1}{2}c^2(m_\mu{}^2-M_1{}^2)m_\mu{}^2$	
1	−1	1		$m_\mu{}^2$
1	0	1	$-2m_\mu{}^2t$	$\frac{1}{2}m_\mu{}^2c-m_\mu{}^2(M_0{}^2-M_1{}^2+t)-2m_\mu{}^2(m_\mu{}^2-M_0{}^2)$
1	1	1	$-m_\mu{}^2ct$	$-\frac{1}{2}cm_\mu{}^2(2m_\mu{}^2-M_0{}^2-M_1{}^2+t)$

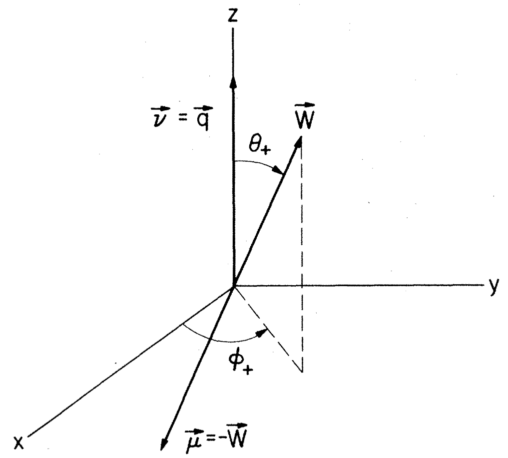

FIG. 25. μ-W_0 center-of-mass–system coordinates, where $\vec{\nu}=\vec{q}$ and $\vec{\mu}=-\vec{W}$; $\vec{p}$ and $\vec{p}_0$ lie in the xz plane; θ_+ is the polar angle of the W_0 and ϕ_+ the azimuthal angle of the W_0.

and

$$H=\frac{G}{8\pi\sqrt{2}}\,\alpha^2\frac{1}{E_\nu^{\,2}}=\frac{6.61\times10^{-39}}{E_\nu^{\,2}}\ \mathrm{GeV}^2\,\mathrm{cm}^2\,. \tag{A32}$$

If the muon mass is neglected, the integrand in Eq. (A31) can be expressed simply in terms of dot products. The integrand for $m_\mu=0$ is given in Table VIII. The integrations proceed as follows:

(i) The integrand is independent of ϕ_p; therefore this integration merely introduces a multiplicative factor of 2π.

(ii) The ϕ_+ dependence is contained in the $(\mu\cdot P)$ and $(W\cdot P)$ terms; the explicit dependence is

$$(W\cdot P)/m=-2g_2\xi+(\nu_1+\nu_2)-(1/|\alpha|)g_3^{1/2}(\alpha^2\Gamma^2-\xi^2)^{1/2}\cos\phi_+ \tag{A33}$$

and

$$(\mu\cdot P)/m=2g_2\xi+(\nu_1-\nu_2)+(1/|\alpha|)g_3^{1/2}(\alpha^2\Gamma^2-\xi^2)^{1/2}\cos\phi_+, \tag{A34}$$

where

$$\nu_1=E_\nu-|\alpha|/2m\,, \tag{A35}$$

$$\nu_2=\nu_1(M_0^{\,2}-m_\mu^{\,2})/2x, \tag{A36}$$

$$g_2=-\nu_1(t-\alpha)/2\alpha^2\,, \tag{A37}$$

and

$$g_3=2x(-t\nu_1^{\,2}/\alpha^2+t/4m^2-1)\,. \tag{A38}$$

This integration is done easily.

(iii) The range for the ξ integration is $(-|\alpha|\Gamma,\ |\alpha|\Gamma)$, which follows from the relation

$$\xi=|\alpha|\Gamma\cos\theta_+\,. \tag{A39}$$

The ξ integration is straightforward but tedious.

(iv) The limits of integration for $|\alpha|$ are given by

$$\alpha_{\min}(t)=\tfrac{1}{2}[\,|t|+(M_0+m_\mu)^2] \tag{A40}$$

and

$$\alpha_{\max}(t)=\tfrac{1}{2}E_\nu[\,t/m+(t^2/m^2-4t)^{1/2}]\,, \tag{A41}$$

the lower limit being determined by the threshold of W_0 production and the upper limit by the constraint of $|\cos\theta_p|\leqslant 1$. In principle, the $|\alpha|$ integration can be done in closed form, but since the $|t|$ integration cannot be done in closed form, both have been performed numerically.

(v) The limits for the $|t|$ integration are

$$t_{\min}=\left(1+\frac{2E_\nu}{m}\right)^{-1}\left(\left\{E_\nu-\left[\left(E_\nu-\frac{1}{2m}(M_0+m_\mu)^2\right)^2-(M_0+m_\mu)^2\right]^{1/2}\right\}^2-\frac{1}{4m^2}(M_0+m_\mu)^4\right) \tag{A42}$$

and

$$t_{\max}=\left(1+\frac{2E_\nu}{m}\right)^{-1}\left(\left\{E_\nu+\left[\left(E_\nu-\frac{1}{2m}(M_0+m_\mu)^2\right)^2-(M_0+m_\mu)^2\right]^{1/2}\right\}^2-\frac{1}{4m^2}(M_0+m_\mu)^4\right). \tag{A43}$$

After the ϕ_+, ϕ_p, and ξ integrations the integrand can be expressed as

$$\frac{d^2\sigma}{d|t|d|\alpha|}=\frac{H}{|\alpha|t^2}\Psi_2(t)\left(\sum_{i=0}^{3}R_{ijk}S_{ijk}+\sum_{i=1}^{2}R(\beta)_{ijkl}S(\beta)_{ijkl}\right)+\frac{H}{|\alpha|t^2}\Psi_3(t)\left(\sum_{i=0}^{3}F_{ijk}S_{ijk}+\sum_{i=1}^{2}F(\beta)_{ijkl}S(\beta)_{ijkl}\right). \tag{A44}$$

TABLE VIII. The differential cross section $f(|t|,\ |\alpha|,\ \xi,\ \phi_+,\ \phi_p)$ for $m_\mu=0$ in terms of dot products.

$$z^2\Psi_2(t)\{\tau^2[(q\cdot W)^2(2\mu\cdot P\,\nu\cdot P-\mu\cdot\nu P^2)-2q\cdot W\,W\cdot P(\mu\cdot q\,\nu\cdot P+\nu\cdot q\,\mu\cdot P)+(W\cdot P)^2(2\mu\cdot q\,\nu\cdot q-\mu\cdot\nu q^2)]$$
$$+\tau q^2[2q\cdot W(2\mu\cdot P\,\nu\cdot P-\mu\cdot\nu P^2)-2W\cdot P(\mu\cdot q\,\nu\cdot P+\nu\cdot q\,\mu\cdot P)]+q^4(2\mu\cdot P\,\nu\cdot P-\mu\cdot\nu P^2)\}$$

$$+z^2q^2\Psi_3(t)\{\tau^2[-2q\cdot W(\mu\cdot q\,\nu\cdot W+\nu\cdot q\,\mu\cdot W)+W^2(2\mu\cdot q\,\nu\cdot q-\mu\cdot\nu q^2)]$$
$$+\tau q^2[-2q\cdot W\mu\cdot\nu-2(\mu\cdot q\,\nu\cdot W+\nu\cdot q\,\mu\cdot W)]+q^2(-q^2\mu\cdot\nu-2\mu\cdot q\,\nu\cdot q)\}$$

The tensors R, $R(\beta)$, F, and $F(\beta)$ result from the integration of the various terms like

$$(\mu_{\beta} W_{\beta'} + W_{\beta} \mu_{\beta'}) \tfrac{1}{2} \sum_{\text{spin}} v_{\beta} v^{*}_{\beta'} y^j z^k \tag{A45}$$

over ϕ_+ and ξ, and are given in Table IX. It is now straightforward to integrate numerically $d^2\sigma/d|t|d|\alpha|$ to obtain cross sections.

TABLE IX. The tensors F_{ijk}, F_{ijkl}, R_{ijk}, and R_{ijkl} defined in Eq. (A44) resulting from the ξ and ϕ_+ integrations. The limits of integration for the integrals are $(-|\alpha|\Gamma, |\alpha|\Gamma)$.

$$F_{0jk} = 3t \int y^j z^k \, d\xi$$

$$F_{1jk} = \tfrac{1}{4}[M_0^2 t - (M_0^2 - M_1^2 + t)^2] \int y^j z^k \, d\xi + \tfrac{1}{2}(M_0^2 - M_1^2 + t) \int y^j z^{k-1} d\xi - \tfrac{1}{4} \int y^j z^{k-2} d\xi$$

$$F_{2jk} = -\tfrac{1}{2} \int y^{j-1} z^{k-1} d\xi + \tfrac{1}{2}(M_0^2 - M_1^2 - t) \int y^{j-1} z^k \, d\xi - \tfrac{1}{2} t \int y^j z^{k-1} d\xi + \tfrac{1}{2}[t^2 - t(M_0^2 - M_1^2) - 2t(M_1^2 + m_\mu^2)] \int y^j z^k \, d\xi$$

$$F_{3jk} = (m_\mu^2 t - \tfrac{1}{4} t^2) \int y^j z^k \, d\xi + \tfrac{1}{2} t \int y^{j-1} z^k \, d\xi - \tfrac{1}{4} \int y^{j-2} z^k \, d\xi$$

$$F_{1jkl} = [M_0^2 t - \tfrac{1}{4}(M_0^2 - M_1^2 + t)^2] \int y^j z^k w^l \, d\xi + \tfrac{1}{2}(M_0^2 - M_1^2 + t) \int y^j z^{k-1} w^l \, d\xi - \tfrac{1}{4} \int y^j z^{k-2} w^l \, d\xi$$

$$F_{2jkl} = -\tfrac{1}{2} \int y^{j-1} z^{k-1} w^l \, d\xi + \tfrac{1}{2}(M_0^2 - M_1^2 - t) \int y^{j-1} z^k w^l \, d\xi - \tfrac{1}{2} t \int y^j z^{k-1} w^l \, d\xi + \tfrac{1}{2}[t^2 - t(M_0^2 - M_1^2) - 2t(M_1^2 + m_\mu^2)] \int y^j z^k w^l \, d\xi$$

$$R_{0jk} = P^2 \int y^j z^k \, d\xi$$

$$R_{1jk} = (a_1^2 - \tfrac{1}{2} b_1^2) \int y^j z^k \xi^2 \, d\xi - 2a_1 a_3 \int y^j z^k \xi \, d\xi + (a_3^2 + \tfrac{1}{2} b_2) \int y^j z^k \, d\xi$$

$$R_{2jk} = (b_1^2 - 2a_1^2) \int y^j z^k \xi^2 \, d\xi + 2a_1(a_3 - a_2) \int y^j z^k \xi \, d\xi + (2a_2 a_3 - b_2) \int y^j z^k \, d\xi$$

$$R_{3jk} = (a_1^2 - \tfrac{1}{2} b_1^2) \int y^j z^k \xi^2 \, d\xi + 2a_1 a_2 \int y^j z^k \xi \, d\xi + (a_2^2 + \tfrac{1}{2} b_2) \int y^j z^k \, d\xi$$

$$R_{1jkl} = (a_1^2 - \tfrac{1}{2} b_1^2) \int y^j z^k w^l \xi^2 \, d\xi - 2a_1 a_3 \int y^j z^k w^l \xi \, d\xi + (a_3^2 + \tfrac{1}{2} b_2) \int y^j z^k w^l \, d\xi$$

$$R_{2jkl} = (b_1^2 - 2a_1^2) \int y^j z^k w^l \xi^2 \, d\xi + 2a_1(a_3 - a_2) \int y^j z^k w^l \xi \, d\xi + (2a_2 a_3 - b_2) \int y^j z^k w^l \, d\xi$$

$$a_1 = (\alpha + 2mE_\nu)(t - \alpha)/(2\alpha^2)$$

$$a_2 = [x - \tfrac{1}{2}(M_0^2 - m_\mu^2)](-\alpha - 2mE_\nu)/(2x)$$

$$a_3 = [x + \tfrac{1}{2}(M_0^2 - m_\mu^2)](-\alpha - 2mE_\nu)/(2x)$$

$$b_1 = \left[2x\left(\frac{-tE_\nu(mE_\nu + \alpha)}{m\alpha^2} - 1\right)\right]^{1/2} \frac{m}{\alpha}$$

$$b_2 = b_1^2 \alpha^2 \Gamma^2$$

$$w = 1/(q^2 + 2q \cdot W)$$

*Work supported in part by the U. S. Atomic Energy Commission. Prepared under Contract No. AT(11-1)-68 for the San Francisco Office, U. S. Atomic Energy Commission.

†Present address: Department of Physics, Stanford University, Stanford, Calif. 94305.

[1] T. D. Lee, Phys. Rev. Letters 25, 1144 (1970).

[2] The conventions used in this paper are as follows: The metric is $(1, -1, -1, -1)$; spinors are normalized such that $u^\dagger u = 2E$; the Dirac matrices are

$$\gamma_0 = \begin{bmatrix} 1 & 0 \\ 0 & -1 \end{bmatrix}, \quad \gamma_i = \begin{bmatrix} 0 & \sigma_i \\ -\sigma_i & 0 \end{bmatrix}, \quad \gamma_5 = \begin{bmatrix} 0 & 1 \\ 1 & 0 \end{bmatrix};$$

$\not{p} = \gamma_\mu p_\mu$ and $e^2 = 4\pi\alpha$.

[3] A. C. T. Wu and C. P. Yang, Phys. Rev. D 1, 3180 (1970).

[4] D. H. Coward *et al.*, Phys. Rev. Letters 20, 292 (1968).

[5] J. S. Bell and M. Veltman, Phys. Letters 5, 94 (1963). Equation (5) is in error; the corrected term should read $-\tfrac{1}{2}(|Q|/2K_f)^3$.

[6]In all our coherent calculations we assume a simple exponential charge distribution rather than the possibly more realistic Fermi distribution to calculate the form factor. As a result, our coherent cross sections are too large. Near threshold our results are too large by an order of magnitude and well above threshold our results are about 20% larger than those done assuming a Fermi charge distribution. Near threshold the coherent cross section is a negligible part of the total cross section and thus is unimportant. In general, because of the severe κ dependence of the cross sections, choice of coherent form factors is a matter of preference.

[7]R. Linsker, Columbia University Report No. NYO-1932(2)-199, 1971 (unpublished).

[8]J. Reiff, Nucl. Phys. B28, 495 (1971).

[9]The data for W_1-production cross sections are taken from R. W. Brown and J. Smith [Phys. Rev. D 3, 207 (1971)] and also from calculations done by P. J. Oddone, in NAL Report No. 21 (unpublished).

[10]The value of $M_1 = 37.29$ GeV/c^2 was included since T. D. Lee has recently proposed this value for the W_1 mass [T. D. Lee, Phys. Rev. Letters 26, 801 (1971)].

[11]The data here for W_1 production used in comparison with W_0 production are taken from R. W. Brown and J. Smith, Ref. 9, and also from P. J. Oddone (private communication).

[12]These data for W_1 production used in comparison with W_0 production are from R. W. Brown, R. H. Hobbs, and J. Smith, Phys. Rev. D 4, 794 (1971).

[13]For a more quantitative explanation, see J. S. Bell and M. Veltman, Phys. Letters 5, 151 (1963).

[14]The q^2 in this section should not be confused with the electromagnetic $q^2 = t$ mentioned earlier. W production can be considered from the point of view of neutrino inelastic scattering, and then q^2 is the momentum transfer squared at the lepton vertex, which is equal to $|(\nu - \mu)^2|$.

[15]D. Cline, A. K. Mann, and C. Rubbia, Phys. Rev. Letters 25, 1309 (1970).

[16]The results presented in this paper are for elastic and coherent production only. The inelastic process will increase the total cross section, but should be characterized by the same qualitative behavior in its differential distributions. This follows since the distributions depend most critically upon which diagram dominates and not the details of the hadronic electromagnetic vertex.

[17]G. Bernardini *et al.*, Nuovo Cimento 38, 608 (1965).

[18]C. H. Llewellyn Smith, Nucl. Phys. B17, 277 (1970).

[19]C. G. Callan, Jr. and D. J. Gross, Phys. Rev. Letters 22, 156 (1969). Here Callan and Gross define their scaling functions $F(x)$ differently. The relation in the text is from D. J. Gross and C. H. Llewellyn Smith, Nucl. Phys. B17, 277 (1970).

[20]See, for example, E. D. Bloom *et al.*, MIT-SLAC Report No. SLAC-PUB-796, 1970 (unpublished), presented at the Fifteenth International Conference on High Energy Physics, Kiev, U.S.S.R., 1970.

[21]J. Reiff (private communication).

PHYSICAL REVIEW D VOLUME 5, NUMBER 3 1 FEBRUARY 1972

Search for New Vector Mesons by Diffractive Photoproduction at the National Accelerator Laboratory

A. I. Sanda
National Accelerator Laboratory, Batavia, Illinois 60510

and

A. Wijangco
Department of Physics, Columbia University, New York, New York 10027

(Received 16 August 1971)

If an as yet unobserved vector meson exists, it can be seen most easily by diffractive photoproduction on nuclei using a photon beam at the National Accelerator Laboratory (NAL). We have considered the problem of coherent production of such a particle on nuclei, taking into account the mixing between the ρ and the new vector meson to arbitrary order. The method used here can be generalized to describe coherent scattering of hadrons and nuclei. It will be shown that the interference effect reduces the production of the new vector meson considerably and that the A dependence of the production cross section plays an important role.

INTRODUCTION

In order to formulate the concept of vector-meson dominance, it is crucial to know whether or not there are other vector mesons besides the ρ, ω, and ϕ through which the photon interacts with hadrons. Since ρ, ω, and ϕ are produced diffractively when a high-energy photon beam strikes a nucleus, we expect such mesons to also be photoproduced diffractively. The diffractive production has the advantage that the produced particle must have quantum numbers similar to those of the pho-